ABSTRACT

THE STRUCTURE AND STABILITY OF EXPANDING AND CONVERGING NEAR-STOICHIOMETRIC FLAMES

by
Raymond Addabbo

The stability of expanding and converging premixed flames is investigated theoretically. These configurations are inherently unsteady and represent simple examples of positively (expanding) and negatively (converging) stretched flames. A new model is employed in this study that incorporates both hydrodynamic and diffusional-thermal effects. The model expands earlier works by incorporating variable transport properties, variations in the mixture strength and a more realistic dependence on viscosity.

The expanding flame is shown to remain stable at small radii provided the thermal diffusivity exceeds the mass diffusivity of the deficient reactant. However, once the flame achieves a critical size, a cellular instability appears, consistent with experimental observations. The effects of viscosity and equivalence ratio on the onset of instability as well as the subsequent development of a cellular structure is studied. Theoretical predictions are given for critical flame size, cell size and growth rate of a disturbance. It is shown that, as the flame continues to expand indefinitely, there is an ever increasing range of unstable wavelengths. This cascade is fractal in nature and a fractal analysis is pursued that results in an expression for the turbulent flame speed. Results are shown to be in good agreement with experiments.

The converging flame is shown to be unconditionally unstable to disturbances of all wavelength. This instability is attributed to thermal expansion. The contracting surface area of this negatively stretched flame serves to enhance the growth rate of a disturbance. For this configuration, it is shown that diffusive-thermal effects are secondary to hydrodynamic effects, even at small radii.

THE STRUCTURE AND STABILITY OF EXPANDING AND CONVERGING NEAR-STOICHIOMETRIC FLAMES

by
Raymond Addabbo

A Dissertation
Submitted to the Faculty of
New Jersey Institute of Technology
and Rutgers, The State University of New Jersey - Newark
in Partial Fulfillment of the Requirements for the Degree of
Doctor of Philosophy in Mathematical Sciences
Department of Mathematical Sciences
Department of Mathematics and Computer Science, Rutgers - Newark

August 2001

APPROVAL PAGE

THE STRUCTURE AND STABILITY OF EXPANDING AND CONVERGING NEAR-STOICHIOMETRIC FLAMES

Raymond Addabbo

Dr. John K. Bechtold, Dissertation Advisor — Date
Associate Professor of Mathematical Sciences, NJIT

Dr. Michael Booty, Committee Member — Date
Associate Professor of Mathematical Sciences, NJIT

Dr. Dawn Lott, Committee Member — Date
Assistant Professor of Mathematical Sciences, NJIT

Dr. Jonathan H. C. Luke, Committee Member — Date
Professor of Mathematical Sciences, NJIT

Dr. Moshe Matalon, Committee Member — Date
Professor of Engineering Sciences and Applied Mathematics,
and Mechanical Engineering, Northwestern University

BIOGRAPHICAL SKETCH

Author: Raymond Addabbo

Degree: Doctor of Philosophy

Date: August 2001

Undergraduate and Graduate Education:

- Doctor of Philosophy in Mathematical Sciences
  New Jersey Institute of Technology, Newark, NJ, August 2001
- Master of Science in Applied Mathematics
  New Jersey Institute of Technology, Newark, NJ, October 1998
- Master of Science in Mathematical Sciences
  New York University, NYC, NY, January 1994
- Master of Science in Physics
  Fairleigh Dickinson University, Teaneck, NJ, May 1982
- Bachelor of Science in Science
  Fairleigh Dickinson University, Teaneck, NJ, October 1980

Major: Mathematical Sciences

This thesis is dedicated to my wife Darla without her this thesis would not have been possible, and to my two daughters Darlayne Ann and Rayna Marie who are both a constant source of inspiration and joy.

ACKNOWLEDGMENT

Many thanks must go to my advisor, Dr. Bechtold, not only for his interest and enthusiasm for this work but also for all his support and encouragement. The members of my dissertation committee, Dr. Booty, Dr. Lott, Dr. Luke and Dr. Matalon are to be thanked not only for their careful review of this work, but also for their time and interest. Dr. Blackmore's discussions on fractals have been very helpful and he is to be acknowledged for sharing his insights. Dr. Tilley is to be thanked for his interest in this work. Dr. Ahluwalia, Chairperson of the Mathematics Department, is to be thanked for all of his support and encouragement.

The graduate students help make the NJIT Math Department very special. Many thanks go to Dr. Walker, Dr. James, Mr. Kunec, Mr. Tran and Dr. Chen for all their help, and to my classmate Ms. Antoniou for her interest in combustion.

Thanks go to Dr. Yefet for sharing his insights.

My colleagues at the College of Aeronautics have been very supportive of me over the years. Particular thanks must go to Andrew Grossfield, Ph.D., P.E., Chairperson of Basic Science, for his support and accommodating to my schedule. My colleague and friend, Prof. LaVergne is to be thanked for all his help and support. Dr. Belonzi, Prof. Scalise and Prof. Arcidiacono, P.E., are to be thanked for reminding me of the importance of a sense of humor. Dr. Fitzpatrick, President of the College of Aeronautics, is thanked for his support.

Dr. Alex Simos can never be thanked enough.

My Mom Joan and my Dad Remo have alway been there for me and to them I owe a special thank you.

TABLE OF CONTENTS

Chapter **Page**

LIST OF TABLES

LIST OF FIGURES

NOMENCLATURE

$A(T)$ ..... Amplitude of Disturbance

$B(T)$ ..... Coefficient of Velocity

B ..... Chemical Frequency

C_p ..... Specific Heat at Constant Pressure

$C(T)$ ..... Coefficient of Pressure

$D(XT)$ ..... Solution of Velocity

D_i ..... Mass Diffusivity

E ..... Activation Energy

$F(r, \theta, \varphi)$ ..... Parametric Position of the Flame

$G(t)$ ..... Coefficient of Pressure

H ..... Enthalpy

I_i ..... Transport Constants

J_i ..... Coefficients of $O(\delta)$ Amplitude

L_D ..... Thickness of Thermal-Diffusion Zone

ℓ ..... Deviation of Lewis Number from Unity

Le ..... Lewis Number

Ma ..... Mach Number

$\mathbf{n}$ ..... Normal to the Flame Surface

P ..... Pressure

Pr ..... Prandtl Number

Q_i ..... Solutions to $O(\delta)$ Amplitude

R^o ..... Gas Constant

$R(t)$ ..... Flame Radius

S_f^0 ..... Adiabatic Flame Speed

S_f ..... Flame Speed

T ..... Temperature

T ..... Scaled Time

t ..... time

$V = (u, v, w)$ ..... Velocity

W_i ..... Molecular Weight

Y_i ..... Mass Fraction

Greek Symbols

α ..... Markstein Parameter

α_i ..... Solutions to Velocity and Pressure

δ ..... Relative Flame Thickness

ϵ ..... Thickness of Reaction Zone

κ ..... Flame Stretch

λ ..... Thermal Conductivity

μ ..... Viscosity

ν_i ..... Stoichiometric Coefficients

ν_n ..... Normal Velocity of the Flame Surface

ρ ..... Density

σ_{ij} ..... Deviatoric Stress Tensor

σ ..... Thermal Expansion

τ^- ..... Stress Tensor

κ ..... Flame Stretch

Φ ..... Equivalence Ratio

Φ ..... Potential

ϕ ..... Modified Equivalence Ratio

Ω ..... Dimensionless Reaction Rate

ω ..... Growth Rate

$\dot{\omega}$ ..... Arrhenius Reaction Rate

CHAPTER 1
INTRODUCTION

The interaction of a premixed flame with its underlying flow field is a complicated process that is of practical importance in many applications. A partial list of important technological areas where these interactions play a key role includes internal combustion engines, rocket engines, materials processing, furnaces and accidental fires. Although planar flames in uniform flows have been widely studied, both theoretically and experimentally, because of their simplicity, flames in practical combustion devices usually involve the propagation of curved flames in unsteady non-uniform flows. The response of premixed flames to these fundamental flow features is the topic to be addressed in this thesis. More specifically, the structure and stability of unsteady curved flames will be examined. The particular geometrical configurations to be investigated are the spherically expanding and converging flames. These configurations have been chosen because they are perhaps the simplest systems that exhibit the fundamental features under investigation. The expanding flame represents a positively stretched flame, i.e. one whose surface area continually increases, while the converging flame is negatively stretched.

One topic to be studied that is of particular interest in combustion science is flame instabilities. The transition from a smooth flame surface to a cellular or wrinkled structure is widely studied by theoreticians and experimentalists. The onset of an instability may be desirable or undesirable, depending on the application. On the one hand, the wrinkling of the flame surface results in an increased surface area which, in turn, increases the consumption rate of fuel. This leads to increased efficiency, and thus engineers often try to induce this type of instabilities in engines and furnaces. On the other hand, the cellular structure leads to complications to experimentalists wishing to measure fundamental flame properties, such as flame speed and temperature. Also, the onset of this instability is often a precursor to

explosions or detonations. In such cases, efforts are made to suppress the instability. One of the goals of this work is to describe the onset of cellular instabilities, and their subsequent development, in expanding and converging flames.

It is well known that premixed flames will develop cellular instabilities when the mass diffusivity of the deficient reactant in the mixture is sufficiently less than the thermal diffusivity of the mixture. This thermo-diffusive instability is caused by the competing effects of heat conduction away from the flame and reactant diffusion towards the flame. It is observed, for example, in lean methane-air mixtures [1] and rich propane-air mixtures [2]. This instability has also been predicted using asymptotic methods. In terms of a Lewis number, Le, defined as the ratio of thermal to mass diffusivities, cells are predicted to form on a flame surface when Le is below a critical value less than unity.

A different type of cellular instability has also been observed in mixtures where the Lewis number is greater than one [3]. Such flames are stable to the thermo-diffusive mechanism discussed above. The cells arise only after the flame has reached a critical size, and the corresponding cell size is observed to be somewhat larger then those attributed to thermo-diffusive effects. The transition from a smooth flame to one with a cellular surface has been observed on spherically expanding flames in rich methane-air [4] and lean propane-air [3] mixtures. In [4], a soap bubble with initial radius of $5cm$ was centrally ignited and cells appeared once the flame reached a size of approximately $1.5cm$. In [3], the propane-air mixture filled a $13cm$-radius spherical vessel and the cellular instability was observed once the flame radius was $7cm$–$10cm$. The cellular instability in these experiments is attributed to hydrodynamic effects, that is the interaction of the flame with the hydrodynamic disturbance it generates via thermal expansion. This mechanism is also responsible for the cells observed in large-scale flames as reported in [5, 6].

Theoretical investigations of the hydrodynamic instability date back to Landau [7] and Darrieus [8] who, independently, treated the flame as a surface of density discontinuity. In their formulation, the density is constant on both sides of the flame surface, although it has a different value on either side. The flow field in both the unburned and burned region are governed by the equations for an inviscid, incompressible flow. The fluid variables on either side are related to one another by imposing conservation of mass and momentum across the front. To close the problem, they also imposed the condition that the front propagates at a constant rate, i.e. they assumed a constant flame speed. Their formulation neglects diffusion entirely and is therefore only appropriate to study disturbances with wavelength significantly larger than the flame thickness. Their model predicts that plane flames are unconditionally unstable. Istratov and Librovich [9] employed this model to study the stability of a spherically expanding flame and they drew a similar conclusion, although they showed that the disturbances grow significantly slower than those on the planar flame owing to the expanding surface.

The most critical assumption of the Landau model was that of a constant flame speed. Markstein [10] proposed that the flame speed should in fact depend on local flame front curvature. Thus, he extended the Landau model by assuming a linear dependence of flame speed on curvature and introduced a phenomenological parameter that presumably contained effects due to flame structure. He showed that short wave instabilities could be stabilized on planar flames, provided his parameter was positive. Istratov and Librovich [9] incorporated Markstein's expression into their model for the spherically expanding flame and found that disturbances could be stabilized during the early stages of propagation, but again only if the Markstein parameter was positive. While these studies suggest that the effects of diffusion in the flame could be a stabilizing factor when the flame is curved, the relation between

Markstein's phenomenological parameter and the physiochemical parameters is not clear.

Recently, asymptotic methods have been employed to systematically analyze the local flame structure and thus derive, rather than prescribe expressions for the flame speed that depend on curvature [11, 12]. These models reveal that the flame speed depends in fact on both curvature and aerodynamic strain, the combined effects known as flame stretch. The dependence is given explicitly in terms of all the physico-chemical parameters in the problem and are free of phenomenological constants. Each of these models incorporate transport effects as a perturbation of the order of the relative flame thickness, and they also provide corrections to the conditions relating mass and momentum on either side of the front. In this way, the stability of both planar [13, 14, 15] and spherically expanding [16] flames has been re-examined. The models have indeed confirmed that the flame structure has a stabilizing effect on short-wave instabilities when the Lewis number exceeds a critical value, Le^*, slightly less than unity. In particular, the results for the spherically expanding flame [16] show that for $Le < Le^*$ the flame experiences a cellular instability immediately after initiation. On the other hand, when $Le > Le^*$, the flame surface remains smooth until a critical radius is reached. The resulting instability is hydrodynamic in nature. The analysis provides explicit expressions for the critical flame size, cell size, and growth rate in terms of all the physical parameters in the problem, including thermal expansion and Lewis number. The analysis also shows that, although viscous effects are retained, the growth rate is independent of Prandtl number, suggesting that viscosity plays a secondary role on stability as compared to diffusion.

In a recent series of papers, Bradley and co-workers [17, 18, 19, 20] have investigated the development of instabilities in explosion flames. They employ the results in [16] as the theoretical framework to interpret their findings. They have found that the rate at which cracks first propagate along the surface of a spherically expanding

flame correlate well with the growth rate of the linear theory. They have also found good qualitative agreement between the theory and their measurements of critical flame radii and cell size. The limiting unstable wavelengths as predicted in [16] also serve as inner and outer cut-offs in Bradley's fractal analysis of large-scale gaseous explosions [20].

Although generally good qualitative agreement between theory and experiment is obtained, quantitative agreement is compromised by some of the assumptions that underly the theories. For example, the theories developed in [11, 12] are single-reactant theories in which one of the species, either fuel or oxidant, appears in very small quantities relative to the others. As such, they are only adequate to describe flame behavior in very lean or very rich mixtures, i.e. mixtures far removed from stoichiometry. Furthermore, the models do not exhibit any dependence whatsoever on mixture strength, usually measured in terms of an equivalence ratio, which is the relative amount of fuel to oxidant in the mixture. The theories have also assumed constant transport properties for convenience in carrying out the calculations, when in fact transport coefficients are known to increase substantially with temperature through the flame zone. This assumption also minimizes the role that viscosity plays on flame stability. Given these simplifications, quantitative predictions that are based on these theories [13, 14] are expected to have limited accuracy. Indeed, the critical flame size at the onset of instability as predicted in [16] are significantly smaller than measured values.

Given the practical importance of expanding flames in both practical applications and fundamental flame studies, new studies are needed that capture more of the real physics of the problem. Recently, a new theory has been developed [21] that allows for variable transport properties and is valid over the full range of mixture strength. In the following, we employ this model to re-examine the stability characteristics of spherically expanding flames. The role of variable transport properties,

mixture strength and viscosity on flame response, including critical flame size, cell size, and growth rate is assessed. It should be noted that the effects of mixture strength [22] and variable transport [23] have been considered previously, but only for the unstretched planar flame.

A spherically expanding flame is initiated by simply igniting a combustible mixture. It is easily produced in experiments and for that reason it is widely studied. On the other hand, the spherically converging flame is very difficult to produce in the laboratory; to do so, one must simultaneously ignite the entire outer shell of a vessel filled with combustible material. Despite this difficulty, converging flames are of both practical and fundamental importance. In intensely turbulent premixed flames, pockets of unburned gas are often formed that are then surrounded and consumed by converging flames [24, 25]. The spherically converging, or imploding, flame has also been identified as the most reliable configuration to measure Markstein parameters in computer simulations. Very little theoretical work has been done on this flame geometry. Sung et. al [26] have employed this configuration and used a diffusional-thermal model to analyze the effect of negative stretch (curvature) on the one-dimensional pulsating instability. As yet, no one has treated the hydrodynamic instability in the presence of negative stretch, and this provides the motivation for some of the work reported here. The model of Bechtold and Matalon [21] is used and a linear stability analysis is pursued.

The thesis is arranged as follows. In the next chapter, the governing equations and reduced models are presented. In chapters 3 and 4 the expanding and converging flames are studied, respectively. Finally, conclusions discussed in Chapter 5.2.

CHAPTER 2

GOVERNING EQUATIONS AND BASIC MODELS

2.1 Introduction

The equations governing premixed flame propagation are very complicated; they consist of equations of heat and mass transport coupled to the Navier-Stokes equations describing the underlying flow. Coupling of the transport equations to the fluids equations occurs through convection, while the coupling in the other direction occurs via density variations through the flame. In addition to the convective non-linearities, the system is further complicated by the highly non-linear reaction rate term. Most practical combustion systems are known to display rapid variation over relatively short spatial and temporal scales, and thus asymptotic methods have proven to be a useful tool to rationally extract reduced models from the full system of equations. The resulting models retain the essential physics of many combustion problems, and can be analyzed to provide an understanding of some very rich phenomena. In this chapter, the most often used reduced models are presented, with a focus on what are termed "hydrodynamic" models. In later chapters, these models will be used to study dynamics of expanding and converging flames.

2.2 Governing Equations

A premixed flame is a chemically reacting front that propagates through a combustible mixture. We will assume that chemistry occurs via a one step irreversible reaction of the form

$$\nu_F \hat{Y}_F + \nu_O \hat{Y}_O \rightarrow \nu_P \hat{Y}_P, \tag{2.1}$$

with $\hat{Y}_i$ and ν_i the mass fractions and stoichiometric coefficients, where $i = F, O, P$ denote fuel, oxidant and product, respectively. The mixture strength is given in

terms of the equivalence ratio

$$\phi = \frac{\hat{Y}_{F_u}/\nu_F W_F}{\hat{Y}_{O_u}/\nu_O W_O}, \tag{2.2}$$

where Y_{i_u} denote the mass fractions in the fresh mixture and W_i is the molecular mass. To avoid discussing lean and rich mixtures separately, we define the related parameter

$$\Phi = \frac{\hat{Y}_{E_u}/\nu_E W_E}{\hat{Y}_{D_u}/\nu_D W_D}, \tag{2.3}$$

where the subscripts E and D denote excess and deficient reactants, respectively. As defined, Φ is always greater than unity, it is equal to the equivalence ratio for fuel rich mixtures and the reciprocal of the equivalence ratio for lean mixtures.

As the flame front moves into a region of lower temperature (unburned region), there is a convective flux of species in the direction from the unburned to burned region and diffusion of heat in the opposite direction. The energy equation, written in terms of the temperature, $\hat{T}$, has the form

$$C_p\hat{\rho}\frac{\hat{D}\hat{T}}{\hat{D}\hat{t}} - \hat{\nabla}\cdot\left(\tilde{\lambda}\nabla\hat{T}\right) = \frac{\hat{D}\hat{P}}{\hat{D}\hat{t}} + \Phi + Q\dot{\omega}, \tag{2.4}$$

where P is the pressure, ρ is the density, Φ is the viscous dissipation (the conversion of kinetic energy into thermal energy), $\tilde{\lambda}$ is the thermal conductivity, C_p is the specific heat at constant pressure, Q is the heat release and $\frac{\hat{D}}{\hat{D}\hat{t}} = \frac{\partial}{\partial\hat{t}} + \hat{\mathbf{V}}\cdot\hat{\nabla}$, is the convective derivative. The reaction rate term obeys an Arrhenius law, and for a two-reactant mixture has the form

$$\dot{\omega} = \hat{\rho}Y_F Y_O B e^{-E/R^o\hat{T}}. \tag{2.5}$$

Here B is the chemical frequency, $Y_i = \hat{Y}_i/W_i$ are the mass fractions, and R^o is the gas constant. The equations describing the transport of reactants through the flow field are

$$\hat{\rho}\frac{\hat{D}Y_i}{\hat{D}\hat{t}} - \hat{\nabla}\cdot\left(\hat{\rho}D_i\hat{\nabla}Y_i\right) = -\nu_i\dot{\omega}, \tag{2.6}$$

where D_i is the mass diffusivity of species i. Note that the term $Q\dot{\omega}$ on the right hand side of (2.4) represents the amount of heat generated by the chemical reaction and is positive since we have an exothermic reaction, while the term $\dot{\omega}$ on the right hand side of (2.6) represents the consumption of species and is therefore negative. The flow field is governed by the Navier-Stokes equations for a viscous, compressible fluid, i.e.

$$\frac{\partial \hat{\rho}}{\partial \hat{t}} + \hat{\nabla} \cdot (\hat{\rho}\hat{\mathbf{V}}) = 0 \tag{2.7}$$

and

$$\hat{\rho}\frac{\hat{D}\hat{\mathbf{V}}}{\hat{D}\hat{t}} = -\hat{\nabla}\hat{P} + \hat{\nabla} \cdot \hat{\sigma}_{ij}, \tag{2.8}$$

where $\hat{\sigma}_{ij}$ is the deviatoric stress tensor given as

$$\hat{\sigma}_{ij} = 2\hat{\mu}\left(\hat{d}_{ij} - \frac{1}{3}\hat{\nabla} \cdot \hat{\mathbf{V}}\right) \quad \text{with} \quad \hat{d}_{ij} = \frac{1}{2}\left(\frac{\partial \hat{u}_i}{\partial \hat{x}_i} + \frac{\partial \hat{u}_j}{\partial \hat{x}_j}\right) \tag{2.9}$$

and $\hat{\mu}$ is the kinematic viscosity. Finally, we assume an ideal gas and write the equation of state

$$\hat{P} = \hat{\rho}R^o\hat{T}. \tag{2.10}$$

To nondimensionalize the above equations, temperature, density and pressure will be referred to their values in the fresh mixture far upstream. The adiabatic flame speed, S_f^0, will be chosen as the characteristic velocity, and lengths will be scaled on the characteristic length scale associated with the bulk flow, L. This may be, for example, the size of the combustion chamber, a burner radius, or the curvature of the flame front. The time scale is L/S_f^0. Note that diffusion also introduces a length scale, $L_D = \hat{\lambda}_u/\rho_u c_p S_f^0$, which determines the flame thickness, where $\hat{\lambda}_u$ is the value of the thermal conductivity $\hat{\lambda}$ far upstream. The above equations can now be written in the the following form

$$\frac{\partial \rho}{\partial t} + \nabla \cdot (\rho\mathbf{V}) = 0, \tag{2.11}$$

$$\rho\Big\{\frac{\partial \mathbf{V}}{\partial t} + (\mathbf{V}\cdot\nabla)\mathbf{V}\Big\} = -\frac{1}{\gamma Ma^2}\nabla P + \delta Pr\nabla\cdot\sigma_{ij}, \tag{2.12}$$

$$\rho\Big\{\frac{\partial Y_i}{\partial t} + (\mathbf{V}\cdot\nabla)Y_i\Big\} - \delta Le_i^{-1}\nabla\cdot(\lambda\nabla Y_i) = -\delta\Omega\nu_i, \tag{2.13}$$

$$\rho\Big\{\frac{\partial T}{\partial t} + (\mathbf{V}\cdot\nabla)T\Big\} - \delta\nabla\cdot(\lambda\nabla T) = \frac{\gamma-1}{\gamma}\Big\{\frac{DP}{Dt} + \gamma Ma^2\delta Pr\Phi\Big\} + \delta q\Omega \tag{2.14}$$

and

$$\rho T = P. \tag{2.15}$$

The parameters appearing here include $\gamma = C_p/C_v$ with C_v the specific heat at constant volume, the Mach number $Ma = \frac{S_f^0}{\sqrt{\gamma\hat{P}_u/\hat{\rho}_u}}$, the Prandtl number $Pr = \frac{\hat{\mu}_u C_p}{\hat{\lambda}_u}$ and the Lewis number, which is the ratio of thermal to mass diffusivities i.e. $Le_i = \hat{\lambda}_u/\hat{\rho}\hat{D}_i C_p$. In writing these equations, temperature-dependent transport coefficients were assumed, i.e. $\lambda = \hat{\lambda}/\lambda_u = \lambda(T)$, although Prandtl and Lewis numbers were assumed constant. The parameter $\delta = L_D/L$ represents the relative thickness of the flame, and in many practical situations it is quite small, i.e. $\delta \sim 10^{-2}$. Note, however, that when the flame is highly curved or the outer flow is highly non-uniform, δ may be $O(1)$.

Of interest in this work are premixed flames which propagate much slower than the speed of sound (typically $S_f^0 \approx 40cm/s$). For such flames, the Mach number is extremely small and it follows from the momentum equation that P is independent of spatial variables. We, therefore, invoke the isobaric approximation and expand P as $P(x,t) = 1 + \gamma Ma^2 p(x,t)$, such that the first term on the right hand side of (2.14) vanishes and the equation of state also simplifies. Furthermore, the momentum equation now depends only on the disturbed pressure, $p(x,t)$. The resulting simplified equations from (2.12), (2.14) and (2.15) are

$$\rho\Big\{\frac{\partial \mathbf{V}}{\partial t} + (\mathbf{V}\cdot\nabla)\mathbf{V}\Big\} = -\nabla p + \delta Pr\nabla\cdot\sigma_{ij}, \tag{2.16}$$

$$\rho\Big\{\frac{\partial T}{\partial t} + (\mathbf{V}\cdot\nabla)T\Big\} - \delta\nabla\cdot(\lambda\nabla T) \;=\; \delta q\Omega, \tag{2.17}$$

and

$$\rho T = 1. \tag{2.18}$$

These equations (2.16)–(2.18) along with (2.11) and (2.13) serve as the starting point for a number of reduced models. The system as it stands is still very complicated, and no exact solutions exist, even for simple flame-flow configurations. As mentioned earlier, the complications can be attributed to the full coupling of the transport and fluids equations, and the nonlinear reaction rate term. Both these issues can be dealt with in a formal asymptotic way; the former by considering the thin flame limit, $\delta \to 0$, and the latter by exploiting the limit of large activation energy, $E \to \infty$. The reduced models that result from these tactics will now be discussed in turn.

2.3 Landau-Darrieus Model

One of the earliest theoretical treatments of premixed flames was given independently by Landau [7] and Darrieus [8], who examined the linear stability of a planar flame. They considered an infinitely thin flame, i.e. a surface at $x = f(y,z,t)$, thereby neglecting effects of reaction and diffusion. The equations they used can formally be obtained by setting $\delta = 0$ in (2.13), (2.16) and (2.17). In particular, the transport equations for a single reactant mixture

$$\rho\Big\{\frac{\partial Y}{\partial t} + (\mathbf{V}\cdot\nabla)Y\Big\} \;=\; 0, \;\; x \neq f \tag{2.19}$$

and

$$\rho\Big\{\frac{\partial T}{\partial t} + (\mathbf{V}\cdot\nabla)T\Big\} \;=\; 0, \;\; x \neq f \tag{2.20}$$

determine that T and Y remain constant along particle paths and thus,

$$T = \begin{cases} 1 & \text{unburned} \\ \sigma & \text{burned} \end{cases} \tag{2.21}$$

and

$$Y = \begin{cases} Y_u & \text{unburned} \\ 0 & \text{burned.} \end{cases} \tag{2.22}$$

From the equation of state, the density also attains a constant value on either side of the flame. In this approach, the flame is regarded as a surface of density discontinuity separating burned from unburned gas. It can be expressed mathematically as $F(\mathbf{X}, t) = x - f(y, z, t) = 0$, and for definiteness we choose $F > 0$ to correspond to the burned region. A unit normal pointing toward the burned region can be written as $\mathbf{n} = \frac{\nabla F}{|\nabla F|}$, and the normal velocity of the surface is given as $\nu_n = -\frac{F_t}{|\nabla F|}$. The flow field on either side of the flame surface is now governed by the equations for an inviscid, incompressible fluid,

$$\nabla \cdot \mathbf{V} = 0 \tag{2.23}$$

and

$$\rho\Big\{\frac{\partial \mathbf{V}}{\partial t} + (\mathbf{V} \cdot \nabla)\mathbf{V}\Big\} = -\nabla p, \tag{2.24}$$

although the density assumes different constant values on the two sides. The solutions on either side must be related to each other across the front. Landau and Darrieus imposed conditions of mass and momentum conservation across the front, i.e. the Rankine-Hugoniot relations. Employing the notation $[\Phi] = \Phi^{(Burned)} - \Phi^{(Unburned)}$, these conditions can be written as

$$[\rho(\mathbf{V} \cdot \mathbf{n} - \nu_n)] = 0, \tag{2.25}$$

$$[\mathbf{V} \times \mathbf{n}] = 0 \tag{2.26}$$

and

$$[p + \rho \mathbf{V} \cdot \mathbf{n}(\mathbf{V} \cdot \mathbf{n} - \nu_n)] = 0. \tag{2.27}$$

These relations can be obtained by directly integrating the mass and momentum equations across a surface, or alternatively by treating the flame as a boundary layer and using asymptotic methods to do a local analysis of the flame zone. Both derivations are presented in Appendix A and Appendix B. Finally, with three components of velocity, one component of pressure and the location of the flame front to be solved for and only four jump conditions, an additional condition is needed to close the problem. Landau assumed the difference between the velocity of gas in the fresh mixture and the speed of the moving front was constant, giving the flame speed equation

$$S_f \equiv \mathbf{V} \cdot \mathbf{n} - \nu_n \;=\; 1. \tag{2.28}$$

The above model is written in a coordinate-free form, and has been used to investigate premixed flame behavior in various geometries. Landau [7] and Darrieus [8], however, only applied their model to study the stability of a planar flame. They considered a stationary planar front, i.e. $f = 0$, with a uniform stream of combustible mixture supplied at $x = -\infty$. The velocity is readily found to be

$$\mathbf{u}^* = \begin{cases} \mathbf{i} & x < 0 \\ \sigma\mathbf{i} & x > 0. \end{cases} \tag{2.29}$$

Upon perturbing the system, they found that there always exists an unstable mode with growth rate given by

$$\omega = -\frac{\sigma}{\sigma+1}k + \frac{\sqrt{\sigma(\sigma^2+\sigma-1)}}{\sigma+1}k. \tag{2.30}$$

A second root is negative and does not provide information about instabilities. This result, which tells us that planar flames are always unstable, is contradicted by experiments, where planar flames under certain conditions are shown to be stable. Landau's result does give us insight into the nature of flame instability, namely that the hydrodynamic instability is due to the thermal expansion of the gases in the mixture as the flame propagates from a region of low density to high density.

It should also be pointed out that in a laboratory there is often stabilizing effects present, such as heat loss to walls and burners, flame front curvature, straining in the flow field, etc.

2.4 Diffusional-Thermal Model

The Landau model discussed in the previous section describes large flames whose thickness is much smaller than the characteristic length scale of the flow. Thus, for example it is appropriately used to study long wave instabilities for which the wave length of a disturbance is much larger than the diffusion length. In many practical systems, however, the characteristic dimension of the flow field is of the same order of magnitude as the flame zone, i.e. $\delta = 1$, and thus diffusion and convection are of comparable magnitude. To analyze these systems researchers often employ the so-called diffusional-thermal, or constant density, model. While this model will not be employed in this thesis, a brief description of it is given here for completeness.

The full system of equations (2.11), (2.12) and (2.16)–(2.18) with $\delta = 1$ is very complicated for two reasons. First, the reaction rate term is highly nonlinear, and second, there is full coupling between the transport equations and the equations of hydrodynamics. Both of these issues can be dealt with in a formal asymptotic way, the former by considering large activation energy, and the latter by considering weak thermal expansion [27].

Most combustion systems are characterized as having large activation energies, and as a consequence, reaction is confined to a very narrow region in the flow field. Within this narrow region gradients are steep and thus diffusion dominates over convection. On either side of this reaction zone, the reaction rate term is negligible. It vanishes on the burned side because the deficient reactant is entirely consumed, and there exists a state of chemical equilibrium. On the unburned side, the temperature is too low to cause a reaction, and the reaction rate term is exponentially small when

large activation energy is considered. In this region the flow is said to be frozen. By introducing a stretched variable, a local analysis of the reaction zone, where reaction and diffusion balance, can be performed. Asymptotic matching then determines jump conditions that relate the variables on either side. In this way the nonlinear reaction rate term is effectively replaced by jump conditions. Analysis determines that both temperature and species remain continuous across the reaction sheet, while their derivatives have a jump discontinuity. For this reason, this model is sometimes referred to as a δ-function model.

Although the resolution of the reaction zone using this technique of activation energy asymptotics greatly simplifies matters, one still has to contend with the coupling of the equations. However, the equations of hydrodynamics decouple from the transport equations by considering the limit of weak thermal expansion, or essentially constant density. The diffusional-thermal model then consists of having to solve the transport equations for temperature and species (or enthalpy) on either side of a reaction sheet with a prescribed velocity. Solutions on either side are related by imposing the derived jump conditions [27].

The diffusional-thermal model considers the effect of the flow on the flame but ignores the effect of the flame on the flow. Conversely, the Landau, or hydrodynamic, model considers the effect of the flame on the flow, but ignores the effect of flow on flame. Recently, asymptotic methods have been used to derive new models that incorporate both diffusional-thermal and hydrodynamic effects. These models, which are used in this thesis, will now be discussed.

2.5 Hydrodynamic and Diffusional-Thermal Effects

The main criticism of the Landau model is that it ignores the potentially stabilizing effects of diffusion in the flame zone. In order to remedy that situation, Markstein [10] proposed that the flame speed depend on curvature of the front. Thus, he modified

the flame speed equation to include a linear dependence of curvature and inserted a phenomenological parameter as a measure of the sensitivity of this dependence. He showed that, provided this new parameter was positive, curvature can indeed stabilize the flame. Karlovitz [28] later considered a similar phenomenological dependence on both curvature and aerodynamic strain.

In more recent years, asymptotic methods have been used to derive (rather than prescribe) corrections to the flame speed equation (2.28) as well as the jump conditions (2.25)–(2.27) [11, 12]. These models also exhibit an explicit dependence on curvature and strain, the combined effects commonly referred to as stretch, but they are free of phenomenological parameters. In [13] and [15], conditions were derived for a perturbed planar flame, and it was shown that effects of flame structure are stabilizing provided the Lewis number exceeds a critical value. The analysis in [11] resulted in jump conditions that are valid for flames of arbitrary shapes in general fluid flows. The resulting system was expressed in a coordinate-free form [11] that has since been used to study flame dynamics in various configurations [14, 16, 29]. The two earlier theories, [11, 12] are appropriate to describe single-reactant mixtures and thus are only valid when conditions are either very lean or very rich, i.e. off-stoichiometric. The model derived in [21] is more general in that it is valid for both near- and off-stoichiometric mixtures. Furthermore, the model [21] allows for variable transport coefficients, and thus contains a more realistic description of the physics involved.

The theories developed in [11, 12] treat the flame as freely propagating boundary layer. Within this thin layer of $O(\delta)$, a balance is maintained between convection and diffusion. Residing within this flame zone is the yet thinner reaction zone where reaction and diffusion balance. The width of this latter zone is $O(\epsilon\delta)$, where ϵ is proportional to the inverse of the activation energy. Asymptotic methods allow each layer to be analyzed separately, and matching then provides the needed

conditions relating the fluid variables on either side of the flame. To leading order in δ, the Landau model is recovered, as shown in Appendix B. When $O(\delta)$ effects are retained in the perturbation scheme, the resulting model is obtained [21]

$$\nabla \cdot \mathbf{V} = 0, \tag{2.31}$$

$$\rho \frac{D\mathbf{V}}{Dt} = -\nabla p + \delta \hat{\lambda} Pr \nabla^2 \mathbf{V}, \tag{2.32}$$

$$\rho = \begin{cases} 1 & F < 0, \\ \sigma^{-1} & F > 0, \end{cases} \qquad \hat{\lambda} = \begin{cases} 1 & F < 0, \\ \lambda_+ & F > 0, \end{cases} \tag{2.33}$$

and the flame speed equation and jump conditions are

$$\mathbf{V} \cdot \mathbf{n} - \nu_n = 1 - \delta \alpha \kappa, \qquad F = 0^-, \tag{2.34}$$

$$[\rho(\mathbf{V} \cdot \mathbf{n} - \nu_n)] = \delta(\sigma - 1) I_1 \kappa, \tag{2.35}$$

$$[\mathbf{V} \times \mathbf{n}] = \delta \Big\{ -\big(\lambda_+ Pr + \sigma I_1\big)[\nabla \times \mathbf{V}] - (\lambda_+ - 1) Pr\, \mathbf{n} \times \tau^- \cdot \mathbf{n} \Big\} \tag{2.36}$$

$$\begin{aligned} [p + \rho \mathbf{V} \cdot \mathbf{n}(\mathbf{V} \cdot \mathbf{n} - \nu_n)] \;=\; & \delta \Big\{ (\sigma - 1) I_1 \nu_n \kappa + \sigma I_1 [\mathbf{n} \cdot \nabla p] \\ & - (\sigma - 1)\big(\sigma I_1 + I_3\big) \nabla \cdot \mathbf{n} \\ & + Pr\big(2(\sigma - 1)(I_3 - \lambda_+) \nabla \cdot \mathbf{n} \\ & + (\lambda_+ - 1) \mathbf{n} \cdot \tau^- \cdot \mathbf{n}\big) \Big\}. \end{aligned} \tag{2.37}$$

Here

$$\begin{aligned} \mathbf{n} = \frac{\nabla F}{|\nabla F|}, \qquad \nu_n = -\frac{F_t}{|\nabla F|}, \\ \kappa = \nu_n \nabla \cdot \mathbf{n} - \mathbf{n} \cdot \nabla \times (\mathbf{V} \times \mathbf{n})_{F=0^-}. \end{aligned} \tag{2.38}$$

where $\mathbf{n}$ is the unit normal to the flame surface $F(\mathbf{X}, t) = 0$ pointing in the direction of the burned gases, ν_n is the normal velocity of the surface, κ is the flame stretch, and τ^- is the stress tensor evaluated at the upstream edge of the flame. The parameter α is given by

$$\alpha = \sigma I_1 - \frac{\ell(\sigma - 1)}{2} I_2, \tag{2.39}$$

and the constants I_1, I_2 and I_3 can be expressed as

$$I_1 = \frac{1}{\sigma - 1}\int_1^\sigma \frac{\lambda(x)}{x}dx, \quad I_2 = \frac{1}{\sigma - 1}\int_1^\sigma \frac{\lambda(x)}{x}\ln(\frac{x-1}{q})dx, \quad I_3 = \frac{1}{\sigma - 1}\int_1^\sigma \lambda(x)dx.$$

The analysis leading to the above system assumes near unity Lewis numbers and near-stoichiometric mixtures and the following expansions are employed

$$Le_i = 1 + \epsilon\ell_i$$

and

$$\phi = 1 + \epsilon\phi_i,$$

where $\epsilon = T_a^2/R^o E$, with E the activation energy. All effects of Lewis number and stoichiometry are contained in the single lumped parameter

$$\ell = \frac{1}{2 + (\sigma - 1)\phi_1}\left(\ell_E + \ell_D(1 + (\sigma - 1)\phi_1)\right). \tag{2.40}$$

This corresponds to a weighted average of the Lewis numbers of the two reactants. At stoichiometry ($\phi_1 = 0$), the two Lewis numbers are weighted equally and ℓ reduces to the mean value of ℓ_E and ℓ_D. For non-stoichiometric mixtures, the deficient reactant is weighted more heavily, and as conditions move far from stoichiometry $\phi_1 \to \infty$, the effective Lewis number approaches the Lewis number of the deficient reactant. Thus, the single reactant theory is recovered in this limit.

The above system extends the earlier works in [11, 12] in three ways. First, the above system exhibits an explicit dependence on equivalence ratio through the weighted Lewis number. The presence of a single weighted Lewis number reveals that results regarding flame structure and stability from the one-reactant theory apply directly to two-reactant, near-stoichiometric mixtures. Second, we note the presence of an "effective" Prandtl number, $\hat{\lambda}Pr$ in (2.32). Since $\hat{\lambda}$ increases with temperature, it follows that the effective Prandtl number is larger in the burned gases as compared to the unburned gases. Consequently, viscous effects are enhanced. Finally, the jump

conditions (2.34)–(2.37) are also modified as a result of variable transport properties. Note, however, that upon setting $\lambda = 1$, the constants I_1, I_2, and I_3 reduce to

$$I_1 = \frac{\ln \sigma}{\sigma - 1}, \quad I_2 = -\frac{1}{\sigma - 1} \int_{-\infty}^{0} \ln(1 + (\sigma - 1)e^z)\, dz, \quad I_3 = 1,$$

and the constant-transport theory results [16] are recovered, with the only difference being a weighted Lewis number.

The above system is expressed in a coordinate-free form that is useful to study flames of arbitrary shapes in general fluid flows. In the remaining chapters, this system will be employed to investigate the structure and stability of both expanding and converging flames. Of particular interest will be the effects of mixture strength (equivalence ratio) and variable transport properties on the dynamics of unsteady, curved premixed flames.

CHAPTER 3

SPHERICALLY EXPANDING FLAMES

3.1 Formulation

We consider an outwardly propagating flame originating from a point source that propagates into an infinite combustible space. We are concerned with events after the initial transient subsides when the flame obtains a radius R_o that is much larger than the flame thickness, L_D, i.e. $\delta \equiv L_D/R_o \ll 1$. The flame front is described mathematically as $F(r,\theta,\varphi,t) = R(\theta,\varphi,t) - r = 0$, with the normal $\mathbf{n} = \frac{\nabla F}{|\nabla F|}$ pointing toward the burned region as shown in Figure 3.1.

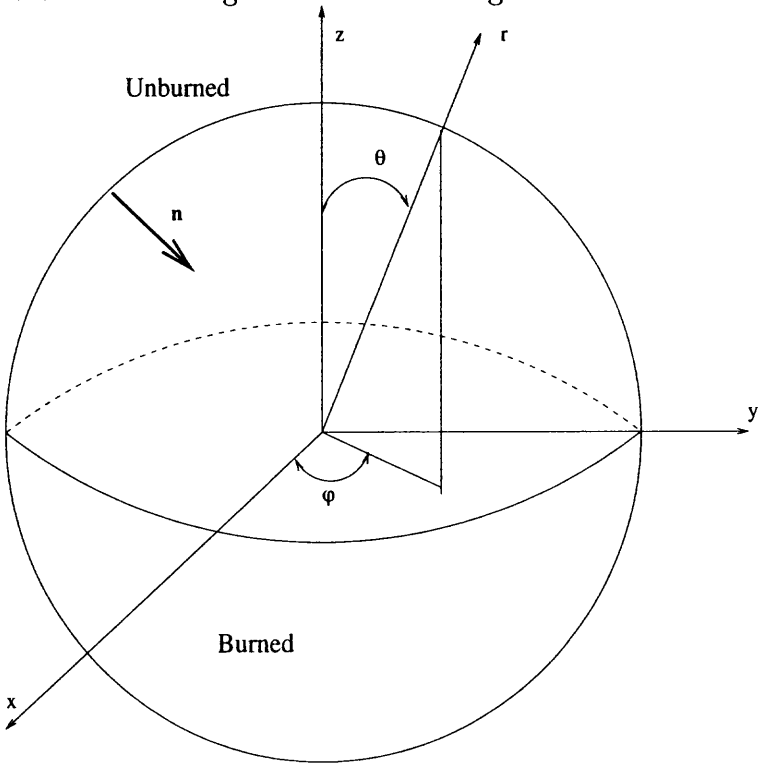

Figure 3.1 Schematic representation of the flame front.

First consider a spherically symmetric flame located at $r = R(t)$, for which there exists a velocity component in the radial direction only. The unit normal, front velocity, and stretch are given by $\mathbf{n} = (-1,0,0)$, $\nu_n = -R_t$ and $\kappa = 2R_t/R$, respectively. The governing equations for this one-dimensional system, which follow

from the general equations presented in Chapter 2 are

$$\frac{\partial(r^2u)}{\partial r} = 0, \tag{3.1}$$

$$\rho\left(\frac{\partial u}{\partial t} + u\frac{\partial u}{\partial r}\right) = -\frac{\partial p}{\partial r} + \delta\hat{\lambda}Pr\left\{\frac{1}{r^2}\frac{\partial(r^2u_r)}{\partial r} - \frac{2u}{r^2}\right\}. \tag{3.2}$$

With the jump conditions given as,

$$-u^* + R_t = 1 - \delta\frac{2\alpha R_t}{R}, \qquad r = R^+, \tag{3.3}$$

$$[\rho(-u^* + R_t)] = \delta\frac{2(\sigma-1)I_1R_t}{R} \tag{3.4}$$

and

$$\begin{aligned}[p^* + \rho u^*(u^* - R_t)] &= \delta\left\{\frac{-2(\sigma-1)I_1R_t^2}{R} - \sigma I_1\left[\frac{\partial p^*}{\partial r}\right]\right. \\ &+ \frac{2(\sigma-1)(\sigma I_1 + I_3)}{R} \\ &- \left.2Pr\left(\frac{2(\sigma-1)(I_3-\lambda_+)}{R} - (\lambda_+ - 1)\frac{\partial u^*}{\partial r}\bigg|_{r=R^+}\right)\right\}.\end{aligned} \tag{3.5}$$

As the flame expands radially outward, the burned gas remains motionless while the flow field generated in the fresh mixture is that of a source flow originating at $r = R(t)$. This follows readily from the conservation equation (2.11), and upon satisfying the jump conditions (3.3) and (3.4), the radial velocity and front velocity are found to be

$$u^* = \begin{cases} 0 & r < R(t) \\ \frac{(\sigma-1)R^2}{r^2} + 2\delta\frac{(\sigma-1)\sigma}{r^2}(\sigma I_1 - \alpha)R_0, & r > R(t), \end{cases} \tag{3.6}$$

$$\frac{dR}{dt} = \sigma + \delta\frac{2\sigma^2}{R_0}[(\sigma-1)I_1 - \alpha]. \tag{3.7}$$

The momentum equation determines the pressure field, which for $r < R$ is

$$\begin{aligned}p^* &= (\sigma-1)\left(1 + \frac{3}{2}(\sigma-1)\right) \\ &+ \frac{\delta(\sigma-1)}{R_0}\left\{-4\sigma I_1 + \sigma(\sigma-1)(2\sigma-1)\ell I_2 + 2I_3 - 4(I_3-1)Pr\right\}\end{aligned} \tag{3.8}$$

and in the region $r > R$ we find

$$\begin{aligned} p^* &= (\sigma-1)\left(\frac{2\sigma R}{r} - \frac{(\sigma-1)R^4}{2r^4}\right) \\ &+ \frac{2(\sigma-1)\sigma}{r}\delta\left\{\sigma\left((3\sigma-2)I_1 - 3\alpha\right) - (\sigma-1)\left(\sigma I_1 - \alpha\right)\frac{R_0^3}{r^3}\right\} \end{aligned} \tag{3.9}$$

The solutions (3.6)–(3.9) are correct to $O(\delta)$. They depend not only on thermal expansion and Lewis number, but also on stoichiometry, variable transport properties and viscosity. The constant transport results [16] are recovered by setting $\lambda = 1$, and in particular the expression for the front velocity takes the form

$$\frac{dR}{dt} = \sigma + \delta\frac{\sigma^2}{R_0}\left[-\frac{2\ln\sigma}{\sigma-1} - \ell\int_{-\infty}^{0}\ln\left(1+(\sigma-1)e^z\right)dz\right], \quad \lambda = 1. \tag{3.10}$$

A more realistic choice for the transport coefficients is [30] $\lambda = \sqrt{T}$, for which the above expression reduces to

$$\frac{dR}{dt} = \sigma + \delta\frac{4\sigma^2}{R_0}\left[\frac{1-\sqrt{\sigma}}{\sigma-1} + \ell\left(\sqrt{\sigma} - 1 + \ln\left(\frac{1+\sqrt{\sigma}}{2}\right)\right)\right], \quad \lambda = \sqrt{T}. \tag{3.11}$$

At large radii, the flame eventually approaches a constant speed, $\frac{dR}{dt} = \sigma$. A typical value of σ is $\sigma \approx 6.0$, and thus the front propagates about six times faster than the adiabatic flame speed, due to the expansion of the burned pocket of gas. The flame propagates faster (slower) than its limiting value, σ, when the Lewis number is less (greater) than the critical value $\ell_c = 2I_1/(\sigma-1)I_2$. This is consistent with the findings of Strehlow [31] who makes the observation that the flame speed of spherically expanding flames in a rich (lean) propane-air mixture is faster (slower) than planar flames in the same mixture. Increasing the mixture strength from lean to rich in propane-air corresponds to a decrease in effective Lewis number, and thus ℓ. In Table 3.1 we compare the critical value of ℓ, calculated using $\lambda = 1$, $\lambda = \sqrt{T}$ and $\lambda = T$ with $\sigma = 6$. The more realistic choice of transport coefficients is seen to result in smaller critical Lewis numbers. Thus, for propane-air mixtures specifically, the transition from faster to slower flame speeds occurs further on the lean side of stoichiometry than predicted by the constant transport case.

Table 3.1 Comparison of results of critical Lewis number for $\sigma = 6$.

	$\lambda_+ = 1$	$\lambda_+ = \sqrt{T}$	$\lambda_+ = T$
ℓ_c	-0.2673	-0.3280	-0.4084

3.2 Linear Stability Analysis

The basic state solution described above is inherently unsteady and therefore two comments are in order regarding stability. First, if a disturbance grows at a rate slower than the flame is expanding then the cells smooth out and the flame is stable to disturbances. If the cells grow faster than the radius of the flame, the cells will propagate over time and the flame is unstable. We therefore must look at the ratio of the disturbance to the radius of the flame in order to determine stability. Second, the linearized perturbation equations will contain information from the basic state and thus they will contain time-dependent coefficients. As a result, disturbances are not expected to grow exponentially in time. Rather, we must seek solutions allowing for arbitrary time-dependent amplitudes and derive a set of ordinary differential equations to determine them.

We introduce small disturbances to the basic state in the following way,

$$\mathbf{v} = \mathbf{v}^*(r,t) + \mathbf{v}'(r,\theta,\varphi,t) \tag{3.12}$$

and

$$p = p^*(r,t) + p'(r,\theta,\varphi,t), \tag{3.13}$$

where the primes are used to denote perturbed variables. The perturbed flame front location is

$$r = R(t)[1 + F(\theta,\varphi,t)], \tag{3.14}$$

so that the growth or decay of F determines whether the flame is stable or unstable. These expressions are inserted into our system (2.11) and (2.16) and the linearized

equations are

$$\nabla \cdot \mathbf{v}' = 0 \tag{3.15}$$

and

$$\rho\left(\frac{\partial \mathbf{v}'}{\partial t} + (\mathbf{v}^* \cdot \nabla)\mathbf{v}') + (\mathbf{v}' \cdot \nabla)\mathbf{v}^*\right) = -\nabla p' + \delta\hat{\lambda}\nabla^2\mathbf{v}' \tag{3.16}$$

Solutions are expressed in terms of spherical harmonic series summed over all possible modes. For example the solution for the perturbed front is sought as

$$F(\theta, \varphi, t) = \sum_{n=0}^{\infty} \sum_{m=-n}^{n} A_{mn}(t) Y_{mn}(\theta, \varphi), \tag{3.17}$$

where $Y_{mn}(\theta, \varphi)$ are the spherical harmonics given by $Y_{mn}(\theta, \varphi) = \Re[e^{im\varphi} P_n^m(\cos\theta)]$, with $P_n^m(\cos\theta)$ the associated Legendre polynomials. For the linear stability analysis, it is sufficient to examine a single mode, and thus for convenience we will drop the summation notation as well as the subscripts on the time-dependent amplitudes. Solutions to the perturbed system are constructed in the burned and unburned regions in the following way. First, in the unburned mixture, the flow remains irrotational to all orders in δ. The velocity is written in terms of a potential Φ as $v' = \nabla\Phi$ and thus we obtain

$$\nabla^2\Phi = 0, \quad \nabla \cdot \mathbf{v} = 0, \tag{3.18}$$

and from (3.16) we obtain

$$\nabla\left[\frac{\partial\Phi}{\partial t} + \mathbf{v}^* \cdot \mathbf{v}' + p'\right] = 0. \tag{3.19}$$

The burned region is treated differently since vorticity is produced at the flame and transported throughout the region. However, since $u^* = 0$ here, taking the divergence of (3.16) yields the simple equation for p' to all orders

$$\nabla^2 p' = 0. \tag{3.20}$$

The velocity field then follows directly from the linearized momentum equation

$$\rho\frac{\partial \mathbf{v}'}{\partial t} = -\nabla p' + \delta Pr\lambda_+\nabla^2\mathbf{v}'. \tag{3.21}$$

The form of these equations suggests that perturbed variables have the form

$$p'(r,\theta,\varphi,t) = P(r,t)Y_{mn}(\theta,\varphi), \tag{3.22}$$

$$\mathbf{v}'(r,\theta,\varphi,t) = \left(u(r,t), v(r,t)\frac{\partial Y_{mn}}{\partial\theta}(Y_{mn})^{-1}, \frac{w(r,t)}{\sin\theta}\right) Y_{mn}(\theta,\varphi), \tag{3.23}$$

and it follows directly from continuity that the fluid variables are related by

$$n(n+1)v = \frac{1}{r}\frac{d}{dr}(r^2u), \quad w = imv. \tag{3.24}$$

Therefore, v and w are immediately known once a solution for u is constructed.

Solutions to the above equations must satisfy the appropriate jump conditions (2.34)–(2.37) that are imposed at a perturbed, moving location. To simplify matters, we will consider a coordinate system attached to the symmetric flame front, i.e.

$$X = r/R(t), \tag{3.25}$$

such that $\frac{\partial}{\partial t} \to \frac{\partial}{\partial t} - R_t\frac{X}{R}\frac{\partial}{\partial X}$. The perturbed front is now located at

$$X = 1 + A(t)Y_{mn}(\theta,\varphi). \tag{3.26}$$

Because disturbances are assumed small, one can apply the jump conditions at the fixed location $X = 1$ by Taylor expanding about this value. Introducing the scaled time

$$T = 1 + \sigma t, \tag{3.27}$$

the linearized jump conditions can be written as

$$u = -\frac{\partial u^*}{\partial X}A + \sigma\frac{d}{dT}(AR) + \delta\alpha\hat{\kappa}, \quad X = 1^+ \tag{3.28}$$

$$[u] = \frac{\partial u^*}{\partial X}A - \frac{1}{2}\delta(\sigma-1)^2\ell I_2\hat{\kappa}, \tag{3.29}$$

$$\begin{aligned}[v] &= u^*A - \frac{\delta}{R_0}\left\{(\lambda_+ Pr + \sigma I_1)\left[v + \frac{\partial v}{\partial X} - u\right]\right. \\ &+ \left. Pr(\lambda_+ - 1)\left(\frac{\partial v}{\partial X} - v + u - 2u^*A + 2\frac{\partial u^*}{\partial X}A\right)\Big|_{X=1^+}\right\}\end{aligned} \tag{3.30}$$

and

$$
\begin{aligned}
[p] &= -\left[\frac{\partial P^*}{\partial X}\right] A \qquad (3.31)\\
&+ \delta\Bigg\{(\sigma-1)(\alpha-\sigma I_1)\hat{\kappa} - \sigma\frac{I_1}{R}\left(\left[\frac{\partial p}{\partial X}\right] + \left[\frac{\partial^2 P^*}{\partial X^2}\right] A\right)\\
&+ \frac{(\sigma-1)}{R_0}(\sigma I_1 + I_3)(n+2)(n-1)A\\
&- \frac{2Pr}{R_0}\left[(\sigma-1)(I_3-\lambda_+)(n+2)(n-1)A - (\lambda_+-1)\left(\frac{\partial u}{\partial X} + \frac{\partial^2 u^*}{\partial X^2}A\right)\Big|_{X=1^+}\right]\Bigg\},
\end{aligned}
$$

where the stretch due to the disturbance is

$$\hat{\kappa} = \left[2\sigma\frac{d}{dT}(AR) + \sigma(n-1)(n+2)A\frac{dR}{dT} - n(n+1)(u^*A+v)\right]R^{-1} \qquad (3.32)$$

evaluated at $X = 1^+$. Solutions to the above system are to be constructed in terms of a power series in δ. By imposing the jump conditions, a coupled system of ordinary differential equations are derived that determine the evolution of the perturbed amplitudes. The perturbation scheme will be carried out to $O(\delta)$ to include both hydrodynamic and diffusional-thermal effects.

We first consider the unburned region, where the solution to the velocity potential (3.18), to all orders in δ is

$$\Phi = B(T)X^{-(n+1)}Y_{mn}(\theta,\varphi). \qquad (3.33)$$

Thus, the three components of the velocity field are given by

$$u = -(n+1)X^{-(n+2)}\frac{B(T)}{R}, \qquad (3.34)$$

$$v = X^{-(n+2)}\frac{B(T)}{R}, \quad w = imX^{-(n+2)}\frac{B(T)}{R} \qquad (3.35)$$

and the pressure is found from (3.19) to be

$$
\begin{aligned}
p &= \Bigg[-\sigma X\frac{dB(T)}{dT} \qquad (3.36)\\
&- \sigma(n+1)\frac{B(T)}{R(T)}\left(\frac{dR(T)}{dT}\right)X + (n+1)u^*(X,T)\frac{B(T)}{R(T)}\Bigg]X^{-(n+2)}.
\end{aligned}
$$

These solutions are also valid to all orders in δ.

Turning now to the burned region, the bounded solution for p from (3.20) is

$$p = C(T)X^n. \tag{3.37}$$

The radial component of velocity is determined from

$$\frac{\partial u}{\partial T} - \frac{X}{R}\left(\frac{dR}{dT}\right)\frac{\partial u}{\partial X} + \frac{1}{R}\frac{\partial p}{\partial X} = \delta\lambda_+ \frac{Pr}{R^2}\left[\frac{\partial^2 u}{\partial X^2} + \frac{4}{X}\frac{\partial u}{\partial X} - \frac{(n-1)(n+2)}{X^2}u\right], \tag{3.38}$$

and the transverse velocity components, v and w follow from (3.24).

3.3 $O(1)$ Stability Results

The leading order solution in the unburned region is given by (3.34)–(3.36) with B_0 and $R = T$. Similarly, the solution for the pressure in the burned region is given by (3.37) with C_0 and $R = T$. To determine the velocity in this region, we turn to (3.38) with $\delta = 0$. The solution of this equation is

$$u_0 = D_0(XT) - nX^{(n-1)}G_0(T) \tag{3.39}$$

and therefore

$$v_0 = \frac{1}{T}\frac{1}{n(n+1)}\frac{\partial}{\partial T}\left(T^2 D_0(XR)\right) - X^{(n-1)}G_0(T), \quad w_0 = imv_0 \tag{3.40}$$

where we have

$$G_0(T) = T^{n-1}\int^T \tau^{-n}C_0(\tau)d\tau. \tag{3.41}$$

Using the solutions (3.34)–(3.36), (3.39) and (3.40) with the flame speed equation (3.28) and the jump conditions (3.29)–(3.31), we find the $O(1)$ system to have the form

$$\mathcal{L}(A_0, B_0, D_0, G_0) = 0$$

with $\mathcal{L}$ written as,

$$\mathcal{L} = \begin{bmatrix} \sigma T^2 \frac{d}{dT} + (3\sigma - 2)T & n+1 & 0 & 0 \\ -\sigma\left(T\frac{d}{dT} + 1\right) & 0 & 1 & -n \\ (1-\sigma)T & -1 & \frac{1}{n(n+1)}\frac{d}{dT}(T^2\cdot) & -T \\ 2(\sigma - 1) & \sigma\frac{d}{dT} + \frac{n+1}{T} & 0 & T\frac{d}{dT} - (n-1) \end{bmatrix}. \quad (3.42)$$

Solving the above system for A_0 results in the differential equation

$$aT^2\frac{d^2A_0}{dT^2} + bT\frac{dA_0}{dT} + cA_0 = 0 \quad (3.43)$$

with

$$a = (\sigma + 1)n + 1,$$

$$b = 2n^2 + (4 + 5\sigma)n + 4$$

and

$$c = -\sigma^{-1}(\sigma - 1)n^3 + 2n^2 + [3(\sigma + 1) - \sigma^{-1}]n + 2.$$

Solving for A_0 we have

$$A_0 = T^\omega \quad (3.44)$$

where ω satisfies the equation

$$a\omega^2 + (b - a)\omega + c = 0. \quad (3.45)$$

There always exists one positive root of the above equation that determines an instability, namely,

$$\omega = \frac{-(b-a) + \sqrt{(b-a)^2 - 4ac}}{2a}. \quad (3.46)$$

The second root is always negative and does not determine an instability. Solutions to the remaining variables are $B_0(T) = \alpha_1 T^{\omega+1}$, $D_0(T) = \alpha_2 T^\omega$ and $G_0(T) = \alpha_3 T^\omega$ with

$$\alpha_1 = \frac{2 - (3 + \omega)\sigma}{n + 1},$$

$$\alpha_2 = \frac{(\sigma - 1)n^2 - (3\sigma + 2\omega\sigma - 1)n - \sigma(\omega + 1)}{1 + \omega - n}$$

and

$$\alpha_3 = \frac{\alpha_2 - \sigma(1+\omega)}{n}.$$

The first observation to point out here is that the amplitude grows as a power law in time as opposed to the exponential growth for the planar flame discussed in Section 2.3, implying that the curvature of the flame has a stabilizing effect. The leading order growth rate, ω, depends only on n and σ and in Figure 3.2 the neutral stability curve is shown in the wavenumber-thermal expansion plane. It is seen that for any $\sigma > 1$ there is always a range of unstable wavelengths. Note, however, that large wavelength disturbances corresponding to $n < 6$ are stable. This is due to the expanding surface. The instability predicted here is a hydrodynamic instability attributed to the thermal expansion of the gas. The stable range is seen to increase indefinitely both as $\sigma \to 1$ and as $\sigma \to \infty$. The former is simply the result of eliminating the mechanism for instability, and the latter occurs because, in this limit, the flame expands infinitely fast so that all disturbances get smoothed out.

This leading order result is expected to be valid at large times when the flame size is much larger than its thickness so that diffusion is negligible. However, at earlier times, and for wavelengths on the order of the flame thickness, diffusion is expected to have a stabilizing effect. These effects are contained in the $O(\delta)$ corrections that we now investigate.

3.4 $O(\delta)$ Stability Results

At this order in the perturbation scheme, the solutions in the unburned region follow from (3.33)–(3.36) with B, and R appropriately expanded to $O(\delta)$. In the burned region, the pressure is again given by (3.37) with C_1. To determine the velocity field in this region, we need to address the inhomogeneous terms that appear in (3.38) at

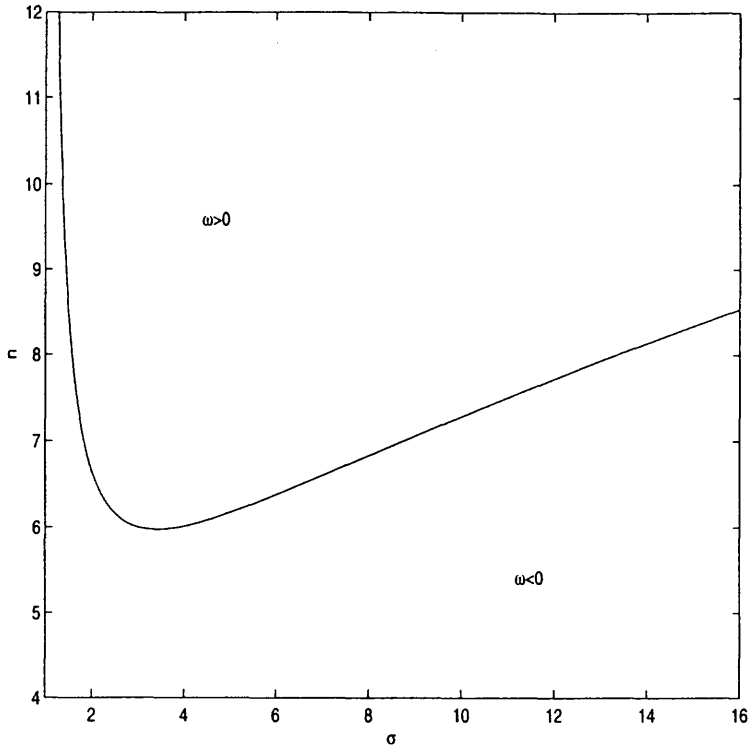

Figure 3.2 Neutral stability curve of the $O(1)$ growth rate.

this order. The solution for u_1 is

$$\begin{aligned} u_1 &= D_1(XR) - nX^{n-1}G_1(T) \\ &+ \left(\ell(\sigma-1)^2 I_2 - 2\alpha\right)\left\{\frac{-\alpha_3 n^2}{(\omega-n)^2}(\omega-n+1)X^{n-1}\right. \\ &+ \left.\left(\omega\alpha_2 X^{\omega} + \frac{n\omega\alpha_3}{\omega-n}X^{n-1}\right)\ln T\right\}T^{\omega-1} \\ &+ \alpha_2\lambda_+ Pr\left(\omega^2+3\omega+2-n(n+1)\right)X^{\omega-2}T^{\omega-1}, \end{aligned} \tag{3.47}$$

where G_1 is defined similar to before with C_0 replaced by C_1. Of course, the solutions for the transverse components, v_1 and w_1 follow directly from (3.24). Imposing the flame speed equation (3.28) and the jump conditions (3.29)-(3.31), we obtain an inhomogeneous form of the system, namely

$$\mathcal{L}(A_1, B_1, D_1, G_1) = N \tag{3.48}$$

with

$$N = \begin{bmatrix} (J_1 + J_1' \ln T)\, T^{\omega} \\ (J_2 + J_2' \ln T)\, T^{\omega-1} \\ (J_3 + J_3' \ln T)\, T^{\omega} \\ (J_4 + J_4' \ln T)\, T^{\omega-1} \end{bmatrix},$$

where J_i and J_i' are given in Appendix C. This system of equations (3.48) can be reduced to a single equation for the amplitude of the flame front, i.e.

$$aT^2 \frac{d^2 A_1}{dT^2} + bT \frac{dA_1}{dT} + cA_1 = (H_1 + H_2 \ln T)\, T^{\omega-1}, \tag{3.49}$$

where H_1 and H_2 are combinations of J_i and J_i' given by

$$\begin{aligned} H_1 &= [2n(n+1) + \omega n\sigma]\,\sigma^{-1} J_1 + n J_1' \\ &+ (n+1)\,[-(\omega+1)J_2 - J_2' + n(n+1)J_3 - nJ_4]\,\sigma^{-1} \end{aligned} \tag{3.50}$$

and

$$\begin{aligned} H_2 &= [2n(n+1) + \omega n\sigma]\,\sigma^{-1} J_1' \\ &+ (n+1)\,[-(\omega+1)J_2' + n(n+1)J_3' - nJ_4']\,\sigma^{-1}. \end{aligned} \tag{3.51}$$

The particular solution of this equation is

$$A_1(T) = \left[\omega\left(\ell q^2 I_1 - \alpha\right) \ln T + Q_1 + \ell Q_2 + Pr Q_3\right] T^{\omega-1}, \tag{3.52}$$

where the constants Q_i depend only on thermal expansion and wavenumber, and have the form

$$\begin{aligned} Q_1 &= \frac{1}{2a\omega + b - 2a}\Big\{ I_1\Big[n^4(\sigma+1) + \sigma n^3(2\omega+5) \\ &+ n^2(\omega\sigma - 2\sigma^2 + \sigma - 1) + n\sigma(\sigma - 7 - 3\omega - \sigma\omega) - 2\sigma(1+\omega)\Big] \\ &+ I_3 n(n^2-1)(n+2)\frac{(\sigma-1)}{\sigma}\Big\}, \end{aligned} \tag{3.53}$$

$$\begin{aligned} Q_2 &= -\frac{(\sigma-1)I_2}{2(2a\omega + b - 2a)}\Big\{ 2n^4 + n^3(2\omega\sigma + 2\omega + 10\sigma - 3) \\ &+ n^2\left[2\sigma\omega^2 + (5\sigma - 1)\omega + 3\sigma - 2\sigma^2 - 2\right] \\ &+ n\left[\sigma\omega^2(1 - 4\sigma) - (14\sigma^2 + 1)\omega + 3 - 9\sigma - 8\sigma^2\right] - 2\sigma(\omega^2 + 4\omega + 3)\Big\} \end{aligned} \tag{3.54}$$

and

$$Q_3 = -\frac{2(\sigma-1)n(n^2-1)}{\sigma(2a\omega+b-2a)}\left[3(\lambda_+-1)+(I_3-\lambda_+)(n+2)\right]. \tag{3.55}$$

Equations (3.44) and (3.52) can now be added to give an expression for the amplitude of the perturbed front correct to $O(\delta)$. This can be written in the convenient form

$$A(R) = A_o R^{\omega(1+\delta\Omega/R\ln R)} \tag{3.56}$$

with

$$\Omega = \frac{Q_1+\ell Q_2+PrQ_3}{\omega}. \tag{3.57}$$

The analysis leading to (3.56) is valid for $\delta \ll 1$, and thus the $O(\delta)$ corrections appearing in the above expression only suggest how diffusional-thermal effects can modify the leading order hydrodynamic instability. Nevertheless, when extrapolated to flame radii on the order of the flame thickness, the above expression provides useful insights into the stability characteristics at early times. Of interest here will be to examine how stoichiometry, variable transport and viscosity can delay or enhance the hydrodynamic instability.

3.4.1 Growth Rate

We first note that for constant transport, $\lambda = 1$, Q_1 and Q_2 reduce to the expressions given in [16, 32], and $Q_3 = 0$. Thus, the effect of viscosity on flame front stability is lost, indicating that the assumption of constant transport properties leads one to underestimate the importance of viscosity on flame front stability. In premixed flames, the diffusion coefficients in fact increase with temperature and thus $\lambda_+ > 1$. For realistic parameter values $Q_1 > 0$ and $Q_2 > 0$ for all n, while $Q_3 > 0$ for all but the first few n implying that viscosity has a stabilizing influence. That is, the amplitude of the disturbance decreases in time when viscous effects are present.

The rate of growth/decay of the disturbance can be determined by

$$\frac{1}{A}\frac{dA}{dR} = \frac{\omega}{R}\left(1-\frac{\delta}{R}\Omega\right). \tag{3.58}$$

Alternatively, Bradley and Harper [17] consider a dimensional growth rate written as

$$\frac{1}{\hat{A}}\frac{d\hat{A}}{d\hat{t}} = \sigma\omega S_f^0\left[1-\frac{2\sigma L_D}{\hat{R}}\left\{\alpha-(\sigma-1)I_1\right\}\right]\left[\frac{1}{\hat{R}}-\frac{L_D\Omega}{\hat{R}^2}\right], \tag{3.59}$$

where $\hat{R}$ is the dimensional radius. For $\Omega < 0$, the growth rate is always positive and the flame is subject to both hydrodynamic and diffusional-thermal instabilities. On the other hand, for $\Omega > 0$, i.e. for ℓ sufficiently large, the growth rate is initially negative and becomes positive after a critical flame size is reached. Therefore, disturbances first decay, then pass through a minimum after which time they grow indefinitely. This is illustrated in Figure 3.3 where the amplitude is shown as a function of time (R) for several values of Ω (corresponding to different Lewis numbers). For a given set of parameters, the disturbance corresponding to a single mode begins to grow before all the others. This mode is expected to determine the cell size observed at the onset of an instability. Our calculations have determined that the first mode to grow corresponds to $n \approx 14$ for a wide range of parameters.

The dimensional growth rate (3.59) is shown in Figure 3.4 as a function of wavelength for several different values of $\hat{R}$ with $\sigma = 5.9$ and $\ell = 1.0055$. These curves are reproduced from Bradley and Harper [17], and are drawn for constant transport properties i.e. $\lambda = 1$ for which the above expression reduces to

$$\frac{1}{\hat{A}}\frac{d\hat{A}}{d\hat{t}} = \sigma\omega S_f^0\left[1-\frac{2\sigma L_D}{\hat{R}}\left\{\alpha-\ln\sigma\right\}\right]\left[\frac{1}{\hat{R}}-\frac{L_D\Omega}{\hat{R}^2}\right]. \tag{3.60}$$

For $\hat{R} < 16.25mm$ the growth rate is always negative and the flame is stable to all wavelengths, but for larger radii (larger times) there always exists a range of unstable wavelengths. Short waves are stabilized by diffusion, while the longest wavelengths are stabilized by stretch, i.e. the expanding surface smoothes out these disturbances. Note that for these parameter values, the constant transport theory predicts a critical wavelength at the onset of instability of approximately $7mm$, and a limiting smaller wavelength of approximately $3mm$ as the flame continues to expand

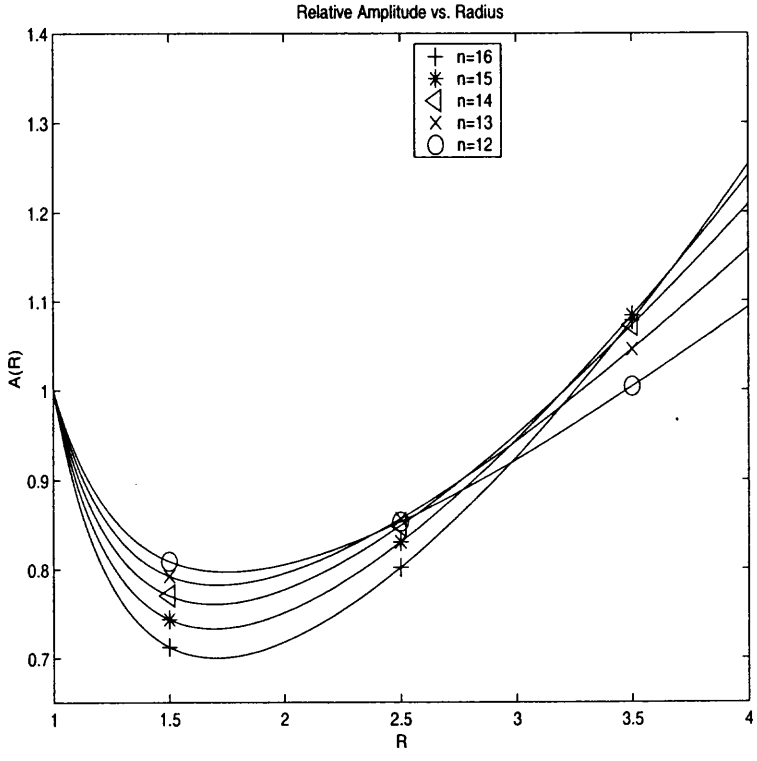

Figure 3.3 Relative amplitude vs. flame position for various n for $\ell = 1.29$ and $\sigma = 6.67$ with constant transport properties.

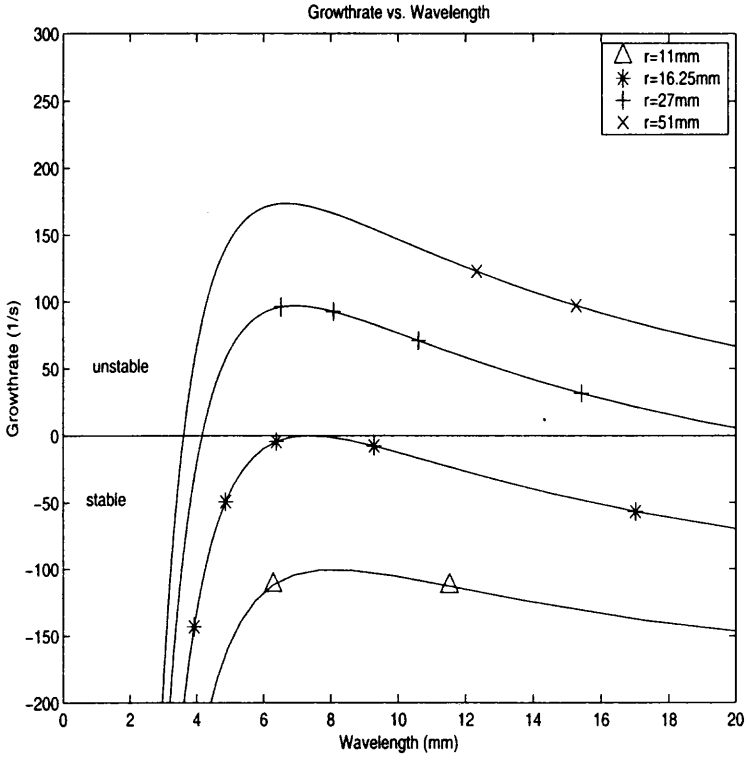

Figure 3.4 Growth rate vs. wavelength for different radii, with $\lambda = 1$, $\ell = 1.0055$, $\sigma = 5.9$, $S_f^0 = 0.4m/s$, and $L_D = 0.05mm$.

indefinitely. In Figure 3.5 we show the growth rate vs. wavelength for $\hat{R} = 20mm$, for different $\lambda(T)$, with the same parameter values used in Figure 3.4. The constant transport theory, $\lambda = 1$ predicts that this flame is unstable. To determine how this conclusion is modified by variable transport, we also show a curve with the same parameters and with $Pr = 0$ and $\lambda = \sqrt{T}$. The new theory predicts a negative growth rate for all wavelengths, and thus the flame is stable at this radius. Of course the hydrodynamic instability will eventually take over, but a more realistic choice of transport coefficients suggests clearly that this instability is delayed until larger radii.

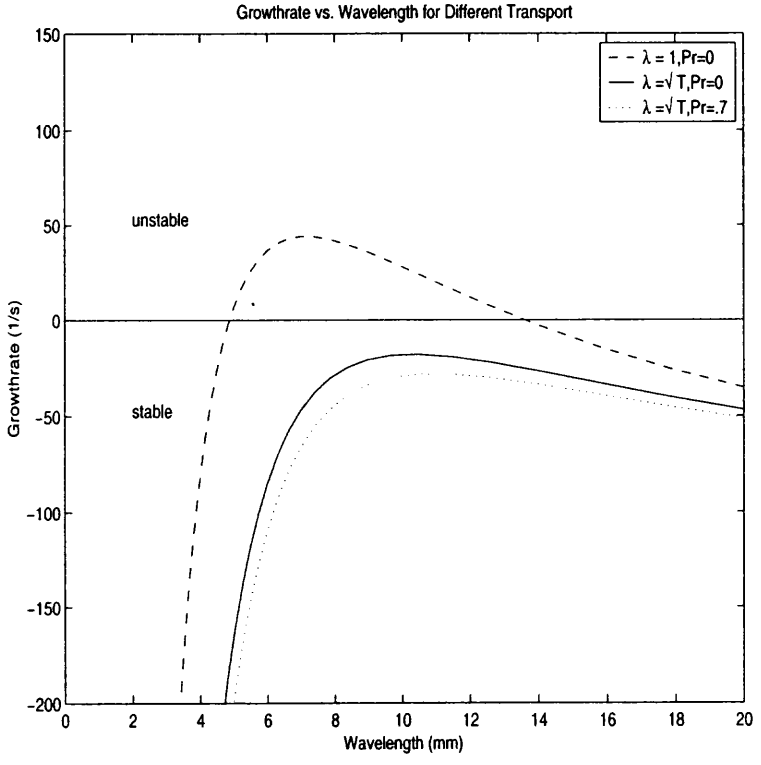

Figure 3.5 Growth rate of instability with $\hat{R} = 20mm$, $L_D = .05mm$, $S_f^0 = 0.4m/s$, $\alpha = 3.5$, $\sigma = 5.9$ with different transport.

Viscosity also tends to stabilize the flame as is seen by the curve in Figure 3.5 with $\lambda = \sqrt{T}$ and the more realistic value of $Pr = 0.7$. The growth rate is clearly less than the inviscid curve for all wavelengths, suggesting a further delay of instability. Finally, the influence of mixture strength on stability is straightforward to

assess, since the dependence on equivalence ratio occurs solely through ℓ. In heavy hydrocarbon-air mixture, such as propane-air, an increase in mixture strength results in a decrease in ℓ, and consequently an increase in the growth rate of a disturbance (recall $Q_2 > 0$). In light hydrocarbons, such as methane, or hydrogen-air, an increase in mixture strength results in an increase in ℓ. Thus, variations in equivalence ratio from lean to rich conditions results in a stabilizing influence for methane-air flames and a de-stabilizing influence for propane-air flames. These predictions are in accord with experimental observations [3] and [4].

3.4.2 Neutral Stability Curves

The onset of an instability can be defined in a number of ways. For example, we may choose the time when the amplitude first returns to its initial value at the onset of instability. Or one could argue that instabilities are not observed until the amplitude achieves a certain magnitude. For definiteness, we define the onset of instability as the point at which the amplitude passes through its minimum and first begins to grow. This point is readily calculated from (3.58) which when set to zero gives

$$\omega\left(1 - \frac{\delta}{R}\Omega\right) = 0. \tag{3.61}$$

In Figure 3.6, we show the neutral stability curves in the n vs. σ plane for several different values of δ/R with $\ell = 1.0$, $Pr = 0$ and $\lambda = \sqrt{T}$. During the early stages of propagation, diffusion stabilizes the flame and a region of instability first develops once the flame has reached a critical size. This unstable region expands as the flame propagates outward, and it approaches the leading order neutral stability curve for large times, i.e. large R.

3.4.3 Critical Flame Size

In Section 3.4.2, (3.61) was used to determine neutral stability curves in the n vs. σ plane for a fixed radius. Alternatively, for fixed σ, (3.61) determines the critical

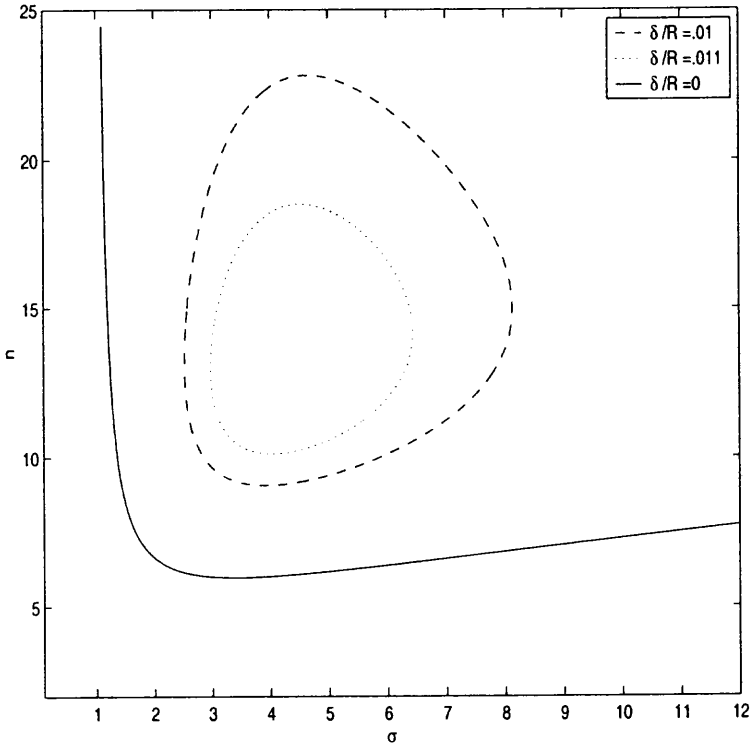

Figure 3.6 Neutral stability curves for $\delta/R = 0, 0.01, 0.011$ and $\ell = 1.0$, $Pr = 0$ and $\lambda = \sqrt{T}$.

radius at the onset of instability as

$$\hat{R} = L_D \Omega. \tag{3.62}$$

In terms of a Peclet number, defined as the ratio of flame radius to thickness and which is a measure of convective to diffusive effects, instabilities arise when

$$Pe \sim \frac{\hat{R}}{L_D} = \Omega. \tag{3.63}$$

Figure 3.7 and Figure 3.8 show the wavenumber n versus critical Peclet number for typical parameter values of rich methane-air and lean propane-air mixtures, which are known to be stable to diffusional-thermal effects. Figure 3.7 is a modification of Figure 4 in [18] in which curves are drawn assuming constant transport coefficients and a single deficient Lewis number. The solid curve shows zero growth rate while the dashed curve shows the maximum growth rate. The curves corresponding to zero growth rate trace out a peninsula, and the nose of each peninsula determines the critical flame size and wavelength at the onset of instability. In all cases, the critical value of n is very close to $n \approx 14$ but the flame size is seen to vary. We also note that as the flame grows to larger radii there is an ever-increasing range of unstable wavelengths, corresponding to more and more cells developing on the expanding surface. The curves shown in Figure 3.8 are drawn for the variable transport case with $\lambda = \sqrt{T}$, for several Prandtl numbers and with Lewis number and thermal expansion the same as the solid curve in Figure 3.7. For the sake of comparison, the solid curve in Figure 3.7 is reproduced in Figure 3.8. The remaining curves assume $\lambda = \sqrt{T}$ and they are seen to lie further to the right, suggesting instability is delayed until a larger flame radius is reached. Similarly, increased values of Pr shift the curves further to the right and we conclude that both variable transport properties and viscosity have a tendency to stabilize the flame. Note that the critical wavenumber at the onset of instability is relatively unchanged. The critical values of Pe are summarized in Table 3.2 for the parameters used in Figure 3.8. Also shown in

Table 3.3 are predicted values with fixed Markstein numbers, $\alpha = 6.4$. Because the Markstein number depends on the choice of transport coefficients, different values of Lewis numbers must be used to maintain a fixed α.

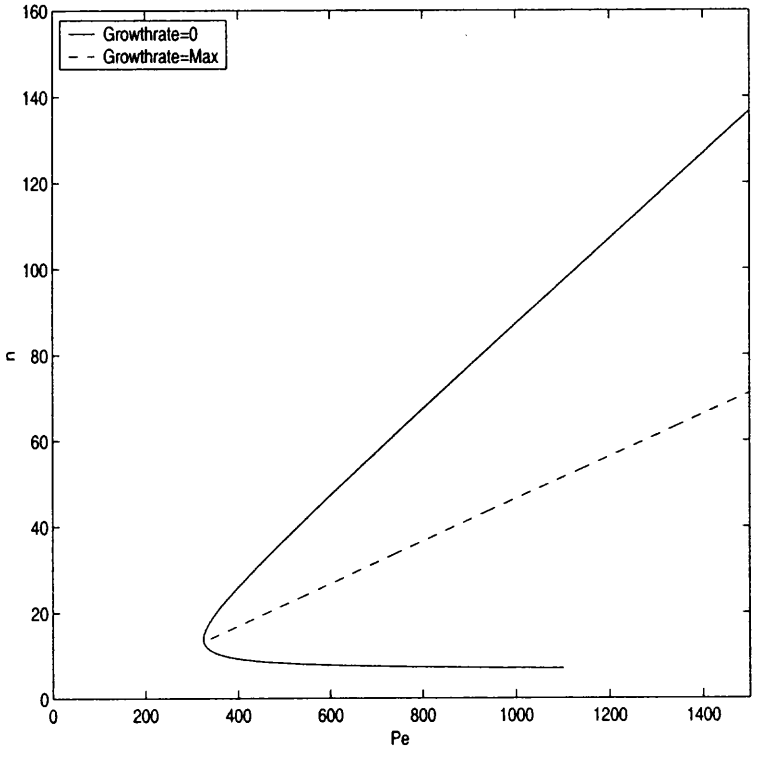

Figure 3.7 n vs. Peclet Number for $\sigma = 6.0, \alpha = 3.5$.

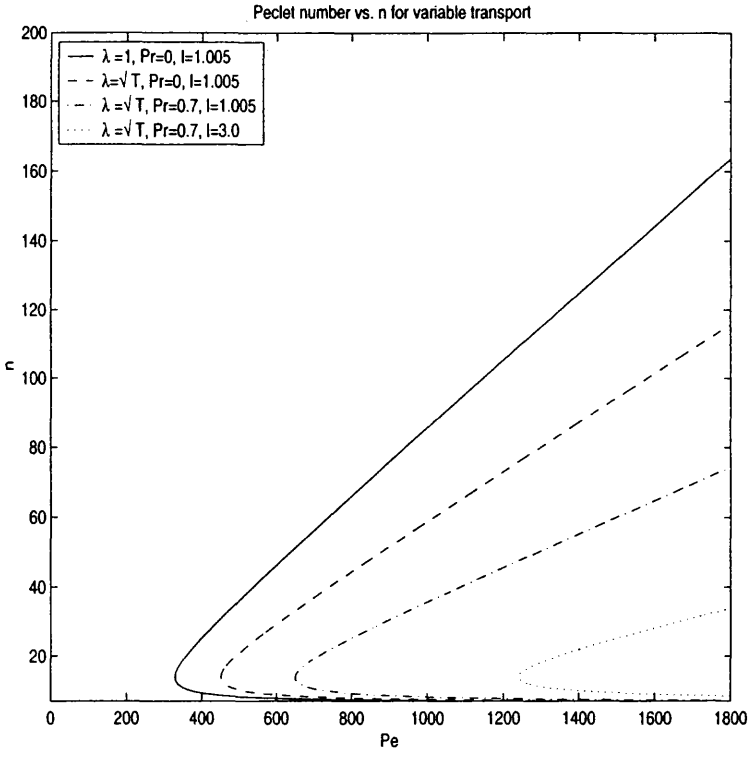

Figure 3.8 n vs. Pe for $\ell = 1.0055$, for different transport properties and viscosity.

We now assess the influence of mixture strength on the flame radius. The dotted curve in Figure 3.8 is drawn with a larger effective Lewis number, $\ell = 3.0$, but with all other parameters held fixed, i.e. $\lambda = \sqrt{T}$ and $Pr = 0$. The larger value of ℓ results in the instability being suppressed. Recall that larger values of effective Lewis number are achieved by increasing mixture strength from lean to rich in light hydrocarbon-air mixtures (e.g. methane-air), or by decreasing mixture strength from

Table 3.2 Critical Pe and cell size ($\sigma = 6$) with $L_D = 0.05mm$.

λ	ℓ	α	Pr	Pe	$\frac{2\pi\dot{R}}{n}$(mm)
1	1.005	3.5	-	330	7.45
$\sqrt{T}$	1.005	5.3	0	452	10.21
$\sqrt{T}$	1.005	5.3	.7	650	14.90
T	1.005	8.5	0.7	1334	31.04
$\sqrt{T}$	3.0	8.9	0.7	1240	28.04

Table 3.3 Critical Pe and cell size ($\sigma = 6$) with $L_D = 0.05mm$.

λ	ℓ	α	Pr	Pe	$\frac{2\pi\hat{R}}{n}$(mm)
1	3.095	6.4	-	800	17.81
$\sqrt{T}$	1.6161	6.4	0	632	14.20
$\sqrt{T}$	1.6161	6.4	.7	831	18.91
T	0.1601	6.4	.7	897	23.49

Table 3.4 Equivalence ratio and critical radius for different propane air mixtures with $\lambda = \sqrt{T}$ and parameter values $\sigma = 5.9$ and $Pr = 0.7$.

Φ	ℓ	$\hat{R}_c(mm)$
0.8	1.43	24.86
1.0	0.875	17.38
1.2	0.37	10.58
1.3	0.27	9.23
1.4	0.21	8.42
1.6	0.13	7.34
1.8	0.080	6.67

rich to lean in heavier hydrocarbon-air mixtures, such as propane-air. Table 3.4 below lists some typical equivalence ratios $\Phi = \nu_O Y_F / \nu_F Y_O$ for a propane-air mixture with their corresponding critical radius.These values were obtained for $\sigma = 5.9$, $Pr = 0.7$ and $L_D = 0.05mm$.

3.4.4 Another Criterion for Instability

The results of the previous sections are based on the definition of instability as the point at which a disturbance first starts to grow. This of course is the earliest possible point to declare an instability. It is quite possible that an instability will not be detected until a disturbance has grown to a certain magnitude, say its initial size. If this latter definition is used for the onset of instability, much larger critical Peclet numbers will be predicted, and all the other results will be modified accordingly.

According to (3.56), a disturbance will return to its initial size when the following condition is satsified,

$$\omega\left(1+\delta\frac{\Omega}{R\ln R}\right)=0. \tag{3.64}$$

In Figure 3.9, we show the resulting modified neutral stability curves in the n vs. Pe plane with $L_D = 0.05mm$ and all other parameters the same as in Figure 3.7. When using this new criterion for instability, R is the appropriate measure of flame size, rather than Peclet number. However, the dashed curve corresponds to the critical conditions that result when the first stability criterion is applied. Clearly, the instability is delayed when the new criterion is used, and we note the onset of instability at $R_c = 37.1mm$ corresponds to a critical Peclet number of $Pe = 742$ using $L_D = 0.05mm$.

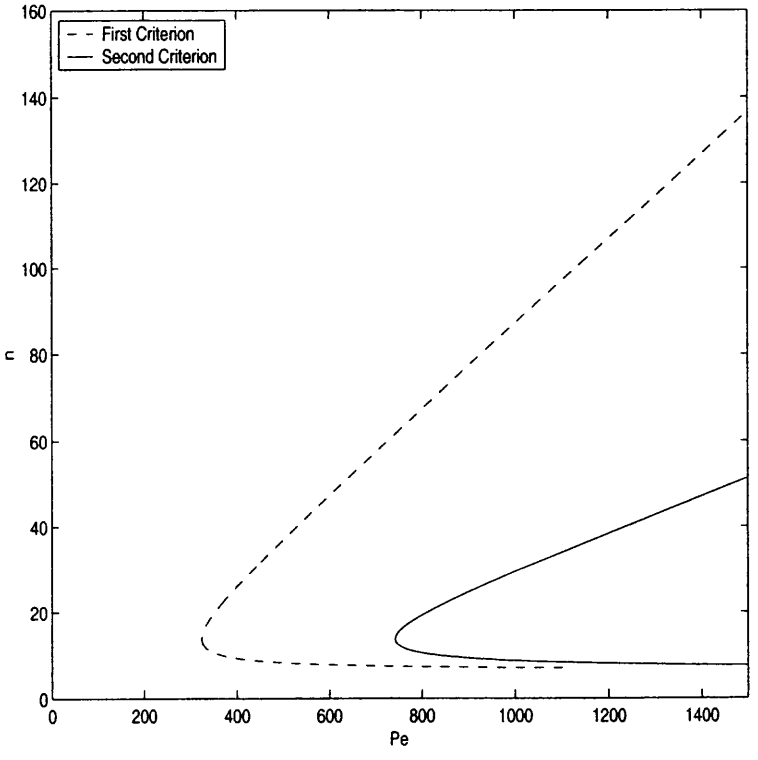

Figure 3.9 n vs. Peclet Number for $\sigma = 6.0, \alpha = 3.5$ for two different stability criteron.

3.4.5 Cell Size

As discussed earlier, as the flame continues to propagate outward after an instability develops, there is an ever-increasing range of unstable wavelengths. The lowest harmonics, corresponding to $n < n_{min}$, are always stabilized by the expanding surface, as shown in Figures 3.6 and 3.7. From (3.57), the limiting value n_{min} for which $R \to \infty$ is found by setting

$$\omega = 0.$$

For a typical value of $\sigma = 6.0$ this gives $n_{min} \approx 6$. Note that this result is independent of Lewis number, Prandtl number and transport coefficients. The stabilizing mechanism here is purely hydrodynamic and is due to stretch. The longest unstable wavelength, which determines the largest expected cell size, is $\hat{\Lambda}_{max} = 2\pi\hat{R}/n_{min}$. Since n_{min} quickly approaches a constant, $\hat{\Lambda}_{max}$ increases with radius as the surface expands. As the flame grows, stretch is weakened and cells of larger size develop.

The top portion of each curve in Figure 3.8 is seen to grow indefinitely and thus more cells are expected to grow on the expanding surface. The curves clearly approach a linear profile, that is Pe/n ~const. Therefore, as the flame expands the wavelength corresponding to the smallest cell size approaches a constant value. Disturbances with wavelength smaller than $\hat{\Lambda}_{min} = 2\pi\hat{R}/n_{max}$ are stabilized by thermo-diffusive effects. The limiting wavelength can be calculated using (3.63) from which we find

$$\begin{aligned} Pe/n \sim & \frac{1}{2\omega_p[(\sigma+1)\omega_p+1]}\Big\{[I_1((\sigma+1)+2\sigma\omega_p)+I_3\frac{\sigma-1}{\sigma} \\ & - \ell(\sigma-1)I_2(1+\omega_p(1+\sigma+\omega_p\sigma)-2Pr(I_3-\lambda_+)(1-1/\sigma)\Big\}, \end{aligned} \tag{3.65}$$

where

$$\omega_p = \frac{1}{\sigma+1}[\sqrt{1+\sigma-1/\sigma}-1]. \tag{3.66}$$

Table 3.5 Minimum unstable wavelength with $L_D = 0.05mm$ and $\sigma = 6.0$

λ	ℓ	Pr	$\hat{\Lambda}_{min}(mm)$
1	1.005	-	3.101
$\sqrt{T}$	1.005	0	4.380
$\sqrt{T}$	1.005	0.7	4.563
T	1.005	0.7	5.860

This cut-off wavelength is identical to the critical wavelength found for perturbed planar flames [33]. In fact, by taking the limits $n \to \infty, R \to \infty$ with R/n held fixed, the spherical flame is locally planar and the stability results regarding planar flames are recovered from (3.56).

The limiting wavelengths for the curves shown in Figure 3.8 are tabulated in Table 3.5. In general, the wavelength of the smallest unstable cell is substantially larger than predicted by the constant-transport theory. This agrees with numerical results of Mukunda [34] who studied the effects of variable transport properties on the stability of planar flames. His results show that variable transport properties substantially enhance the stability, and predicted cell sizes are approximately twice that found using constant transport properties.

Conditions for the development of cells have been reported for a variety of hydrocarbon-air mixtures, using different fuel-oxidant ratios and pressures. Rich methane-air mixtures were studied by Manton, VonElbe and Lewis [35] who report on the existence of cells. Bregeon, Gordon and Williams [36] used rich Hydrogen-air mixtures and report cell sizes of about $10mm$ for near stoichiometric conditions to about $20mm$ for hydrogen rich mixtures. Groff [3] measured cell sizes using lean propane-air mixtures and reports cell sizes ranging from $6.5mm$ to $8.5mm$ with a critical wavenumber between 56 and 100, and a flame radius of about $73mm$. Although his values of the critical radius and the critical wavenumbers are larger than the theoretical predictions, due probably to the different hydrodynamic conditions

in his constant volume vessel, he does obtain good agreement with theoretical predictions of cell size.

The cell sizes reported above are from (3.65) and thus correspond to the smallest cell size that one would expect to observe. However, within the range $n_{min} < n < n_{max}$ there exists a value of n that yields a maximum growth rate. This maximum is shown by the dashed curve in Figure 3.7, which is seen to grow linearly. We can readily calculate the wavelength corresponding to the maximum growth rate by setting to zero the derivative of (3.58) with respect to n. Upon doing this we find that the most unstable wavelength approaches a value that is simply twice the value of the minimum wavelength given in (3.58). We note that the smallest cell size predicted by (3.65) are approximately one half the cell size predicted at the onset of instability. For example, for $\lambda = 1$ and $\ell = 1.0055$, the limiting value of Λ_{min} is $3.101mm$, from Table 3.5 where as the cell size at the onset is approximately $7mm$ as shown in Figure 3.4. This is consistent with the findings of Bradley et al. [40].

3.4.6 Turbulent Flame Speed

As a spherically expanding flame propagates outward, there develops a cascade of decreasing unstable wavelengths. This cascade gives rise to a fractal-like wrinkling of the flame surface as observed by Gostintstev et. al [37] and Filyand et. al [38]. Bradley [19, 20] has proposed that the fractal nature of these flames is very similar to that of turbulence, which is characterized by velocity fluctuations over a range of wavelengths. In his fractal analysis of these flames [17], he employed $\hat{\Lambda}_{min}$ and $\hat{\Lambda}_{max}$ (from the constant transport theory [16]) as the inner and outer cut-off wavelengths to derive an equation for the turbulent flame speed. To compensate for the fact that the constant transport theory underestimates the critical Peclet number at the formation of cells, Bradley [20] proposed that the top portion of the curves in Figure 3.8 be replaced by a line originating at $Pe_{cl} > Pe_c$. The slope of the line

was taken to be less than the limiting slopes shown in Figure 3.8, and both Pe_{cl} and the slope were estimated using correlations with experimental data. The present theory has shown that the critical Peclet number is indeed significantly larger than predicted by the constant transport theory, and thus provides a better estimate for the critical conditions at the onset of flame wrinkling.

Here we follow Bradley [20] and pursue an analytical expression for turbulent flame speed. Consider the flame enclosed in a volume filled with cubes of side a. The fractal dimension, or box dimension, is defined to be

$$D = \lim_{a \to 0} \frac{\ln(N(a))}{\ln(1/a)},$$

where $N(a)$ is the number of cubes of side a that are intersected by the surface. For small a,

$$N(a) \sim (1/a)^D, \quad \text{or} \quad N(a)a^2 \sim (1/a)^{D-2}.$$

For a smooth surface (with $D = 2$) in a unit region,

$$N(a)a^2 \sim 1,$$

and thus for small a, $N(a)a^2$ gives an approximation of the fractal area relative to the area of a smooth surface. For the wrinkled flame, the limiting value of a is determined by the cut-off wavelengths, i.e.

$$a = \hat{\Lambda}_{min}/\hat{\Lambda}_{max} = \frac{n_{min}}{n_{max}},$$

and therefore the area ratio is given by

$$(n_{max}/n_{min})^{D-2}. \tag{3.67}$$

Now let $\hat{R}_w$ denote the mean radius of the wrinkled flame, and $d\hat{R}_w/d\hat{t}$ is the propagation speed of the front. The ratio of the surface area of the wrinkled front to that of a smooth laminar flame at the same radius is given by

$$\frac{d\hat{R}_w}{d\hat{t}} \Big/ \frac{d\hat{R}}{d\hat{t}} = \left(\frac{n_{max}}{n_{min}}\right)^{D-2},$$

where the fractal dimension D will be taken to be 7/3 [19]. Note that $d\hat{R}/d\hat{t} \approx \sigma S_f^0$, and thus the above expression can be written in dimensionless form as

$$\frac{\delta}{\sigma}\frac{dPe_w}{dt} = \left(\frac{n_{max}}{n_{min}}\right)^{1/3}. \tag{3.68}$$

As seen in Figure 3.8, n_{min} rapidly approaches a constant, while n_{max} behaves linearly very soon after the instability sets in. Thus, we consider $n_{min} \approx$ const. and set $n_{max} \approx Pe_c\gamma + c$, where c is a constant related to the size of the flame at the onset of wrinkling, and γ is given by (3.65), i.e.

$$\begin{aligned}\gamma &= \frac{1}{2\omega_p[(\sigma+1)\omega_p+1]}\Bigg\{[I_1((\sigma+1)+2\sigma\omega_p) + I_3\frac{\sigma-1}{\sigma} \\ &- \ell(\sigma-1)I_2(1+\omega_p(1+\sigma+\omega_p\sigma) - 2Pr(I_3-\lambda_+)(1-1/\sigma)\Bigg\},\end{aligned} \tag{3.69}$$

These expressions are inserted into (3.68) and the resulting equation is readily integrated to yield

$$Pe_w = -c/\gamma + \left(\frac{2\sigma\gamma^{1/3}}{3n_{min}^{1/3}\delta}\hat{t}\right)^{3/2}. \tag{3.70}$$

In dimensional form, this gives

$$\hat{R}_w = \hat{R}_w^0 + \left[\left(\frac{2\sigma}{3}\right)^{3/2}\left(\frac{\gamma\hat{\rho}_u c_p}{n_{min}\hat{\lambda}_u}\right)^{1/2} S_L^2\right]\hat{t}^{3/2}, \tag{3.71}$$

where the constant $\hat{R}_w^0$ is the radius at the onset of wrinkling. The turbulent flame speed is now found to be

$$\frac{d\hat{R}_w}{d\hat{t}} = \sigma^{3/2}\left(\frac{2}{3}\frac{\gamma\hat{\rho}_u c_p}{n_{min}\hat{\lambda}_u}\right)^{1/2} S_L^2\,\hat{t}^{1/2}. \tag{3.72}$$

The square root dependence on time correlates well with the turbulent flame speeds measured by Gostintstev et. al [37], as well as those computed by Filyand, et. al [38]. The coefficient of $\hat{t}^{1/2}$,

$$\hat{A}_w = \sigma^{3/2}\left(\frac{2}{3}\frac{\gamma\hat{\rho}_u c_p}{n_{min}\hat{\lambda}_u}\right)^{1/2} S_L^2(\mathrm{m/s^{3/2}})$$

depends explicitly on the physical parameters in the problem. This expression results from the theory developed in [39] for which the flame thickness is based on the

thermal diffusivity. It differs slightly from the expression derived by Bradley [20] who used an expression for flame thickness based on viscosity. Effects of viscosity and Lewis number are in fact contained in γ. In particular, the square root dependence on γ suggests that viscosity decreases turbulent burning velocity. Also, the turbulent velocity is increased by a decrease in ℓ, such as varying mixture strength from lean to rich in propane-air flames. The turbulent velocity will increase indefinitely when ℓ is decreased to a critical value such that $\gamma \to \infty$. This value of ℓ corresponds to the top portion of the curves in Figure 3.8 becoming vertical. For Lewis numbers below this value the flame is always unstable to thermo-diffusive instabilities.

For the parameter values used in Figure 3.8, this coefficient takes on values of approximately $14m/s^{3/2}$. This clearly overestimates the values reported in [37] where values on the order of six or seven were measured for methane-air and propane-air flames. We note that the analysis presented here assumes that the onset of wrinkling corresponds to the onset of turbulence. However, the experiments reported in [37] indicate that the transition to turbulence occurs at a substantially larger Peclet number after wrinkling. Of course, the transition to turbulence is a highly nonlinear phenomenon that can not be captured by the linear analysis presented here. Nevertheless, the analysis provides a reasonable qualitative description of the process.

CHAPTER 4

SPHERICALLY CONVERGING FLAMES

4.1 Formulation

The expanding flame analyzed in the previous chapter represents the simplest configuration of an unsteady, positively stretched flame. Conversely, the spherically converging flame is an example of an usteady, negatively stretched flame; i.e. an element of surface area along the flame surface shrinks as it propagates inward. Whereas the spherically expanding flame is readily produced in the laboratory and is therefore widely studied, the converging flame is not easily produced. To do so would require the instantaneous ignition of a spherical shell surrounding a combustible mixture. Consequently this geometry has received much less attention from researchers. However, it has been recognized as an essential model to describe the burning of pockets of unburned gas, especially as this phenomena occurs in turbulent premixed combustion [26]. Furthermore, it has been suggested to be the most reliable configuration to extract Markstein numbers in computational studies [40]. Here we analyze this flame for hydrodynamic stability.

Consider a pre-existing inwardly propagating flame collapsing into a combustible mixture. The intial radius R_o is much larger than the flame thickness, L_D, i.e. $\delta \equiv L_D/R_o \ll 1$. The flame front is described mathematically as $F(r,\theta,\varphi,t) = r - R(\theta,\varphi,t) = 0$, with the normal pointing toward the burned region, in this case the region outside the flame surface.

Similar, to the expanding flame of Chapter 3, first consider a spherically symmetric flame located at $r = R(t)$, for which there exists a velocity component in the radial direction only. The unit normal, front velocity, and stretch are given by $\mathbf{n} = (1,0,0)$, $\nu_n = R_t$ and $\kappa = 2R_t/R$, respectively. The governing equations for this one-dimensional system, which follow from the general equations presented in

Chapter 2 are

$$\frac{\partial(r^2u)}{\partial r} = 0, \tag{4.1}$$

$$\rho\left(\frac{\partial u}{\partial t} + u\frac{\partial u}{\partial r}\right) = -\frac{\partial p}{\partial r} + \delta\hat{\lambda}Pr\left\{\frac{1}{r^2}\frac{\partial(r^2u_r)}{\partial r} - \frac{2u}{r^2}\right\}. \tag{4.2}$$

The jump conditions are

$$u - R_t = 1 - \delta\alpha 2R_t/R, \qquad r = R^-, \tag{4.3}$$

$$[\rho(u - R_t)] = \delta(\sigma - 1)I_1 2R_t/R, \tag{4.4}$$

and

$$\begin{aligned}[p + \rho u(u - R_t)] \;=\; & \delta\left\{\frac{2(\sigma-1)I_1R_t^2}{R} + \sigma I_1\left[\frac{\partial p}{\partial r}\right]\right. \\ & - 2\frac{(\sigma-1)\left(\sigma I_1 + I_3\right)}{R} \\ & + \left.\frac{4Pr(\sigma-1)(I_3-\lambda_+)}{R} + 2(\lambda_+ - 1)\frac{\partial u}{\partial r}\bigg|_{r=R^-}\right\}.\end{aligned} \tag{4.5}$$

As the flame contracts radially inward, the *unburned* gas remains motionless while the flow field generated in the *burned* mixture is that of a source flow originating at $r = R(t)$. Upon satisfying the jump conditions (4.3) and (4.4), the radial velocity and front velocity are found to be

$$u^* = \begin{cases} 0 & r < R(t) \\ \frac{(\sigma-1)R^2}{r^2} + \delta\frac{2(\sigma-1)R_0}{r^2}[\alpha - \sigma I_1], & r > R(t), \end{cases} \tag{4.6}$$

$$\frac{dR}{dt} = -1 - \delta\frac{2\alpha}{R_0}. \tag{4.7}$$

The momentum equation determines the pressure field, which for $r < R$ is

$$\begin{aligned}p^* \;=\; & \frac{(\sigma-1)(\sigma-3)}{2\sigma} \\ & + \delta\frac{2(\sigma-1)}{R_0}\left\{\alpha - \frac{2\alpha}{\sigma} - \sigma I_1 + I_3\right. \\ & + \left. 2Pr(\lambda_+ - I_3) + 2Pr(\lambda_+ - 1)\right\}\end{aligned} \tag{4.8}$$

and in the region $r > R$ we find using (4.5)

$$\begin{aligned} p^* &= -2\frac{\sigma-1}{\sigma}\left(\frac{R}{r}+\frac{(\sigma-1)R^4}{4r^4}\right) \\ &+ \delta\frac{1}{\sigma}\left\{\frac{(\sigma-1)(-6\alpha+2\sigma I_1)}{r} - \frac{2(\sigma-1)^2R^3}{r^4}(\alpha-\sigma I_1)\right\}. \end{aligned}$$

Note the front velocity dR/dt is negative, and the front propagates at a speed equal to the adiabatic flame speed. This is in contrast to the expanding flame whose radius propagates about six times faster than the adiabatic flame speed, due to the expansion of the burned pocket of gas.

4.2 Linear Stability Analysis

The basic state solution described above is now tested for stability. As for the expanding flame, the unsteady nature of the basic state requires that we look at the ratio of the disturbance to the radius of the flame in order to determine stability. The basic procedure is the same as discussed in Chapter 3, although the method of solution in the respective regions, burned and unburned, differ.

We again introduce small disturbances to the basic state as

$$\mathbf{v} = \mathbf{v}^*(r,t) + \mathbf{v}'(r,\theta,\varphi,t) \tag{4.9}$$

$$p = p^*(r,t) + p'(r,\theta,\varphi,t), \tag{4.10}$$

where the primes are used to denote perturbed variables, and the perturbed flame front location is

$$r = R(t)[1 + F(\theta,\varphi,t)]. \tag{4.11}$$

These expressions are inserted into our system (2.11) and (2.16) and the linearized equations are

$$\nabla\cdot\mathbf{v}' = 0, \tag{4.12}$$

$$\rho\left(\frac{\partial v'}{\partial t} + (\mathbf{v}^*\cdot\nabla)\mathbf{v}' + (\mathbf{v}'\cdot\nabla)\mathbf{v}^*\right) = -\nabla p + \delta Pr\hat{\lambda}\nabla^2\mathbf{v}'. \tag{4.13}$$

For this geometry, it is convenient to work with the vorticity

$$\mathbf{\Omega} = \nabla \times \mathbf{v}, \tag{4.14}$$

and it is noted that

$$\mathbf{\Omega}^* = \nabla \times \mathbf{v}^* = 0. \tag{4.15}$$

Taking the curl of the linearized momentum equation results in the following equation for vorticity

$$\rho\left(\frac{\partial \mathbf{\Omega}'}{\partial t} - \nabla \times (\mathbf{v}^* \times \mathbf{\Omega}')\right) = -\delta Pr\hat{\lambda}\nabla \times \nabla \times \Omega'. \tag{4.16}$$

As before, solutions are expressed in terms of spherical harmonics as

$$p'(r,\theta,\varphi,t) = P(r,t)Y_n^m(\theta,\varphi), \tag{4.17}$$

$$\mathbf{v}'(r,\theta,\varphi,t) = \left(u(r,t), v(r,t)\frac{\partial Y_{mn}}{\partial \theta}(Y_{mn})^{-1}, \frac{w(r,t)}{\sin\theta}\right) Y_{mn}(\theta,\varphi), \tag{4.18}$$

and it follows directly from continuity that the fluid variables are related by

$$n(n+1)v = \frac{1}{r}\frac{d}{dr}(r^2 u), \quad w = imv. \tag{4.19}$$

From (4.14), the three components of vorticity are

$$\mathbf{\Omega}' = \left\{0;\ \zeta\frac{imY_{nm}}{r\sin\theta};\ -\frac{\zeta}{r}\frac{\partial Y_{nm}}{\partial\theta}\right\}, \tag{4.20}$$

where

$$\zeta = u - \frac{\partial(rv)}{\partial r}, \tag{4.21}$$

or, using (4.19)

$$\zeta = u - \frac{1}{n(n+1)}\frac{\partial^2(r^2u)}{\partial r^2}. \tag{4.22}$$

Thus, once a solution for the vorticity is constructed, (4.21) and (4.22) are used to determine u, v and w, and the pressure then follows from the θ-component of the momentum equation. Inserting the expressions (4.21) and (4.22) into the vorticity equation (4.16) yields the following equation for ζ

$$\rho\left(\frac{\partial\zeta}{\partial t} + \frac{\partial(u^*\zeta)}{\partial r}\right) = \delta Pr\hat{\lambda}\left\{\frac{\partial^2\zeta}{\partial r^2} - \frac{n(n+1)}{r^2}\zeta\right\}. \tag{4.23}$$

Solutions to the perturbed system are constructed in the burned and unburned regions in the following way. First, the unburned mixture, enclosed by the sphere, remains irrotational, i.e. $\zeta = 0$, and from (4.22) the radial velocity satisfies the ordinary differential equation

$$r^2\frac{\partial^2 u}{\partial r^2} + 4r\frac{\partial u}{\partial r} + [2 - n(n+1)]u = 0. \tag{4.24}$$

The bounded solution is given by

$$u = G(t)r^{n-1}, \tag{4.25}$$

and solutions for v and p follow from (4.13) and (4.14) as

$$v = \frac{1}{n}G(t)r^{n-1}, \quad p = -r\frac{\partial v}{\partial t}. \tag{4.26}$$

Because the flow is irrotational and the basic state velocity is zero, the above solutions are valid to all order in δ.

In the burned region external to the flame surface, the basic state velocity is not zero and, unlike the case of the expanding flame, it is not possible to decouple a simple equation for p'. Rather, it is more convenient to solve for the vorticity (4.20) and solutions for the velocity components and pressure follow readily.

Adopting a coordinate system attached to the symmetric flame so that the perturbed front location is

$$X = 1 + A(t)Y_n^m, \tag{4.27}$$

the linearized jump conditions can be written as

$$u = \frac{d}{dt}(AR) - \delta\alpha\hat{\kappa}, \tag{4.28}$$

$$[u] = -A\frac{\partial u^*}{\partial X} + \delta(\sigma - 1)\hat{\kappa}\left(\sigma I_1 - \alpha\right), \tag{4.29}$$

$$\begin{aligned}[v] &= -u^*A + \frac{\delta}{R}\left\{(\lambda_+ Pr + \sigma I_1)\left[v + \frac{\partial v}{\partial X} - u\right]\right. \\ &+ \left.(\lambda_+ - 1)Pr\left(u + \frac{\partial v}{\partial X} - v\right)\Big|_{X=1^-}\right\}\end{aligned} \tag{4.30}$$

and

$$
\begin{aligned}
[p] &= -\left[\frac{\partial P^*}{\partial X}\right] A + \delta\Big\{(\alpha - \sigma I_1)2(\sigma-1)\hat{\kappa} \\
&+ \frac{2}{R}\frac{d}{dt}(AR)(\alpha - (\sigma-1)I_1) \\
&+ \sigma I_1 \frac{1}{R}\left(\left[\frac{\partial p}{\partial X}\right] + \left[\frac{\partial^2 P^*}{\partial X^2}\right] A\right) \\
&- \frac{\sigma-1}{R}(\sigma I_1 + I_3)(n+2)(n-1)A \\
&+ \frac{Pr}{R}2(\sigma-1)(I_3 - \lambda_+)(n+2)(n-1)A + Pr(\lambda_+ - 1)\frac{2}{R}\frac{\partial u^-}{\partial X}\Big\},
\end{aligned}
\tag{4.31}
$$

where

$$
\hat{\kappa} = \frac{1}{R}\left(2\frac{d(AR)}{dt} - (n+2)(n-1)A - vn(n+1)\right)_{X=1^-} \tag{4.32}
$$

Solutions to the above system are constructed in terms of a power series in δ. Although the methodology used to construct solutions differs from that used in Chapter 3, the similarities between the cases suggest that the amplitude will evolve according to

$$
A = A_0 R^{\omega(1+\delta\Omega/R\ln R)}. \tag{4.33}
$$

Thus, we seek solutions with time-dependent amplitudes of the form shown above, and by imposing jump conditions, a system of algebraic equations is obtained to determine the growth rates, ω and Ω. It is important to note that the criterion to determine an instability needs to be modified for this problem. The radius is decreasing with time for the converging flame and therefore a disturbance will grow only if the growth rate (i.e. ω at leading order) is negative. Thus, in contrast to most stability analyses, solutions are to be sought with the real part of ω less than zero.

In the unburned region, the solutions are

$$
u = GR^{\omega(1+\delta\Omega/R\ln R)}X^{(n-1)}, \tag{4.34}
$$

$$
v = \frac{1}{n}GR^{\omega(1+\delta\Omega/R\ln R)}X^{(n-1)}, \tag{4.35}
$$

and the pressure is found from (3.21) to be

$$p = -RX\left(\frac{\partial v}{\partial t} - \frac{X}{R}\frac{\partial R}{\partial t}\frac{\partial v}{\partial X}\right). \tag{4.36}$$

In the burned region, a solution for $\zeta(X,t)$ is first sought in the form

$$\zeta(X,t) = R^{\omega(1+\delta\Omega/R\ln R)}\zeta(X), \tag{4.37}$$

which is inserted into (4.23) to obtain an ordinary differential equation for $\zeta(X)$. The solutions for the velocity components and pressure then follow from (4.21), (4.22) and (4.13).

Although the linear stability analysis to follow can be carried out to $O(\delta)$, only the leading order results will be discussed. It will be shown that the converging flame is unstable to disturbances of all wavelengths at leading order. The effects of diffusion, which control the fate of short-wave disturbances, have little or no impact on large wavelength disturbances. Thus, the collapsing flame will be shown to be unconditionally unstable due to hydrodynamic effects.

4.3 Stability Results

The leading order solution in the unburned region is given by (4.34)–(4.36). In the burned region, we first turn to the vorticity equation

$$\frac{d\zeta}{dX}(X + \frac{\sigma-1}{X^2}) - \zeta(\omega + \frac{2(\sigma-1)}{X^3}) = 0, \tag{4.38}$$

whose solution is

$$\zeta = a_2X^2(\sigma - 1 + X^3)^{(\omega-2)/3}. \tag{4.39}$$

The radial component of velocity, u, satisfies (4.23), which takes the form

$$X^2\frac{\partial^2 u}{\partial X^2} + 4X\frac{\partial u}{\partial X} + [2 - n(n+1)]u = -n(n+1)\zeta. \tag{4.40}$$

The bounded solution for u is found to be

$$u = [a_0X^{-n-2} + g(X)]R^{\omega(1+\delta\Omega/R\ln R)}, \tag{4.41}$$

where

$$g(X) = \frac{a_2 n(n+1)}{2n+1}\left\{X^{n-1}\int_X^\infty \eta^{-n+2}(\sigma-1+\eta^3)^{(\omega-2)/3}\,d\eta + X^{-n-2}\int_1^X \eta^{n+3}(\sigma-1+\eta^3)^{(\omega-2)/3}\,d\eta\right\}. \tag{4.42}$$

From (4.19) we find the transverse velocity components; in particular

$$v = \frac{1}{n(n+1)}[X\frac{du}{dX} + 2u]R^{\omega(1+\delta\Omega/R\ln R)} \tag{4.43}$$

and upon inserting into (4.42) this gives

$$v = \frac{1}{n(n+1)}\left[-na_0X^{-n-2} + \frac{a_2(n+1)n}{2n+1}\left\{(n+1)X^{n-1}\int_X^\infty \eta^{-n+2}(\sigma-1+\eta^3)^{(\omega-2)/3}\,d\eta - nX^{-n-2}\int_1^X \eta^{n+3}(\sigma-1+\eta^3)^{(\omega-2)/3}\,d\eta\right\}\right] R^{\omega(1+\delta\Omega/R\ln R)}]. \tag{4.44}$$

The leading order pressure follows from the θ-component of momentum, i.e.

$$p = -\frac{1}{\sigma}\left\{XR\frac{dv}{dt} + (X^2+(\sigma-1)/X)\frac{dv}{dX} + \frac{\sigma-1}{X^2}v\right\}. \tag{4.45}$$

Applying the jump conditions now results in the following system of four algebraic equations to determine A_0, G, a_0 and a_2

$$G = -A_0(\omega+1), \tag{4.46}$$

$$a_0 + \frac{a_2(n+1)}{2}I = A_0(2(\sigma-1)-\omega-1), \tag{4.47}$$

$$-\frac{1}{n+1}a_0 + \frac{a_2 n(n+1)}{2n}I - \frac{1}{n}G = -A_0(\sigma-1), \tag{4.48}$$

$$-\frac{a_0}{\sigma(n+1)}(\omega+\sigma n+\sigma+1) + \frac{a_2(n+1)I}{\sigma(2n+1)} + \frac{\sigma^{(\omega-2)/3}}{n}a_2 - \frac{1}{n}G(\omega-n+1) = -2A_0(\sigma-1) \tag{4.49}$$

where

$$I = \int_1^\infty \eta^{-n+2}(\sigma-1+\eta^3)^{(\omega-2)/3}\,d\eta. \tag{4.50}$$

In order that nontrivial solutions exist to the above system, ω must satisfy the following dispersion relation

$$\beta^2 - n\beta - \frac{n\sigma}{J(\sigma-1)(n+1)}[(\sigma-1)(n-1) + \beta\frac{2n+1}{n}] = 0 \qquad (4.51)$$

where for convenience we have defined

$$\beta = \omega + 1,$$

and the constant J is given by

$$J = \int_1^\infty \eta^{-n+2}\left(\frac{\sigma - 1 + \eta^3}{\sigma}\right)^{(\omega-2)/3} d\eta. \qquad (4.52)$$

The transcendental equation (4.51) has been solved numerically, and curves showing ω vs. n are shown in figure x for several values of σ. The growth rate is found to be negative for all n and any value of σ, and hence the flame is unstable to all wavelengths. It is interesting to note that even in the limit $\sigma \to 1$ for which the mechanism for hydrodynamic instability is suppressed, there is always an unstable root, namely $\omega = -1$. The unsteady nature of this problem requires that all disturbances decay faster than the shrinking flame surface for the flame to be stable. We conclude that spherically converging flames are unconditionally unstable.

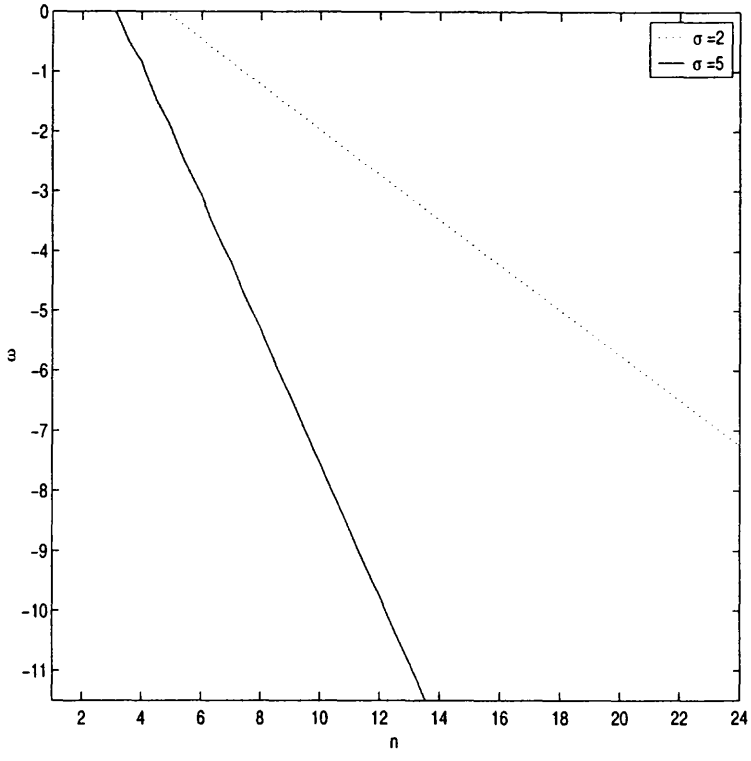

Figure 4.1 Dispersion relation for the converging spherical flame for $\sigma = 2$ and $\sigma = 5$.

CHAPTER 5
SUMMARY OF RESULTS

The structure and stability of expanding and converging flames has been investigated. The outwardly and inwardly propagating spherical flame configurations have been used as they represent the simplest examples of unsteady positively and negatively stretched flames, respectively. Both configurations have important applications in both fundamental flame studies and practical combustion systems.

The unsteady nature of these systems required that the criteria used to determine instability be modified from most other stability analyses. For the flame to be stable, a disturbance must diminish relative to the growing or shrinking front. The expanding surface of the outwardly propagating flame was shown to be a stabilizing factor, while the shrinking surface area of the inwardly propagating flame contributed to instability. In both cases, disturbances were shown to grow according to a power law in time, rather than the more rapid exponential growth found in most studies.

The premixed flame model used in this investigation incorporates both hydrodynamic and diffusional-thermal effects. It is a generalization of earlier theories of flame propagation that treat the flame as a surface of density discontinuity. In contrast to earlier works, the theory employed in this work is valid near stoichiometry and has an explicit dependence on equivalence ratio. It also allows for variable transport properties, and thus allows for the treatment of viscous effects. The effects of mixture strength, viscosity and variable transport on flame stability properties has been examined.

An important element of the work performed here has been to directly compare theoretical predictions to experimental measurements on spherically expanding flames. Most notably, Bradley [20] has investigated the development of instabilities in explosion flames and has correlated experimental findings with theoretical

predictions. However, the theoretical framework he used to interpret is findings was based on earlier models that do not account for variations in mixture strength, transport properties, and viscosity. The present findings are found to clearly provide more accurate predictions of flame properties over a wider range of experimental conditions. Some of the main results will now be summarized.

5.1 Spherically Expanding Flame

The propagation speed of a symmetric spherically expanding flame approaches a constant value as the radius increases indefinitely. The departure from the constant value is largest at earlier times, or smaller radii, when diffusion is important. A critical value of Lewis number was derived which marks the point at which diffusion causes the flame to propagate faster or slower than its limiting value. Realistic transport coefficients were found to result in small values of the critical Lewis number than the constant transport theory predicts. For heavier hydrocarbon-air flames, such as propane-air, the transition from faster to slower propagation speeds occurs further on the lean side of stoichiometry than previously predicted.

All spherically expanding flames will eventually become unstable due to thermal expansion of the gas. However, the expanding surface tends to smooth out the largest wavelength disturbances. Results show the following evolution of the flame. When the Lewis number is sufficiently large, the flame remains smooth for a while and the cellular instability develops only after a critical size is reached. As the flame continues to expand, cells continually sub-divide as more and more wavelengths become unstable. There is a minimum wavelength below which disturbances are stabilized by diffusion. This cascade of decreasing wavelengths has been proposed by Bradley [20] as being reminiscent of fractal-like wrinkling. The results of the present investigation provide explicit expressions form many unstable flame

properties discussed above, including flame size, cell size, growth rate and turbulent flame speed. Some of the main conclusions can be summarized as follows.

Both variable transport properties and viscosity tend to stabilize the flame. They lead to smaller growth rates and a delay in the onset of wrinkling until larger radii are reached. Changing the equivalence ratio from lean to rich conditions results in a stabilizing influence for light hydrocarbon-air flames, such as methane-air, and a de-stabilizing influence for heavy hydrocarbon-air flames, such as propane-air. These predictions are in accord with experimental observations. Neutral stability curves have been drawn by setting the growth rate of a disturbance to zero. Variable transport and viscosity have been shown to yield much larger flame size (or Peclet number) and cell size at the onset of instability.

Once an instability develops, the flame surface evolves into a wrinkled surface with a smallest characteristic cell size. Analytical expressions were given for the smallest unstable wavelength from which minimum cell size was calculated. Variable transport properties were found to yield a larger minimum cell size than that predicted using previous constant transport property results. Viscosity also increased the minimum cell size. In propane-air mixtures the effect of decreasing mixture strength from rich to lean increases the minimum cell size.

The wrinkling of the flame surface is known to be fractal in nature. A fractal analysis has been performed in a manner first proposed by Bradley [20] to obtain an expression for turbulent flame speed. The result predicts that both variable transport properties and viscosity tend to decrease the turbulent burning velocity. The flame speed has a square root dependence on time, in accord with experimental measurements [38].

Most of the main results are obtained by assuming that the onset of instability is associated with the instant at which the amplitude of a disturbance passes through a minimum. This is clearly the earliest possible time to define an instability, and

it is proposed that cells may not become apparent until the amplitude reaches its initial size. Employing this new criterion for instability, the instability is shown to be further delayed.

5.2 Spherically Converging Flame

The converging flame was found to behave much differently from the expanding flame. The propagation speed of the collapsing front was shown to be independent of thermal expansion, and in fact the front propagates at a speed approximately six times slower than the expanding front. A stability analysis was carried out and it was found that the converging flame is unconditionally unstable to disturbances of all wavelength. This result was found to be true for all values of thermal expansion. Whereas the expanding surface of the outward propagating flame tends to smooth out disturbances, the contracting surface of the inward propagating flame enhances the growth rate of a disturbance. Although diffusion may have a tendency to stabilize short wave instabilities, their effects are secondary to hydrodynamic effects, even at small radii.

APPENDIX A

DERIVATION OF THE RANKINE-HUGONIOT EQUATIONS AS AN INTEGRAL ACROSS THE FLAME SURFACE

In this section, the jump conditions (2.25)–(2.27) used in the Landau-Darrieus model will be justified by integrating the hydrodynamic governing equations (2.11) and (2.16) across a small volume element $V(t)$ as shown in Figure A.1.

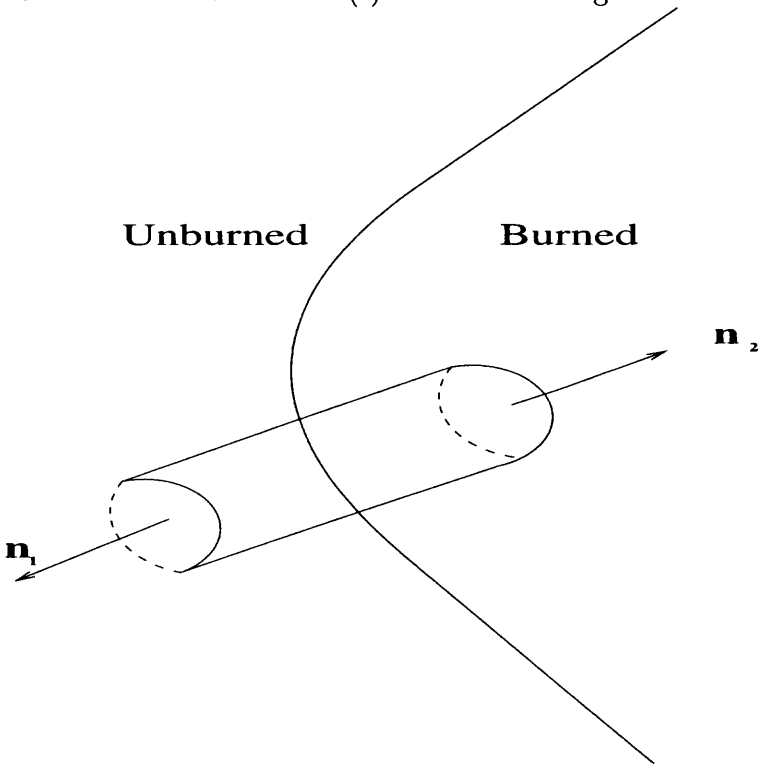

Figure A.1 Volume Element Across the Surface Separating Burned from Unburned Gases.

Integrating the equation of continuity (2.11) over a volume element $V(t)$ we have

$$\int_{V(t)} \rho_t dV + \int_{V(t)} \nabla \cdot (\rho \mathbf{V}) dV = 0. \tag{A.1}$$

We use the expression

$$\frac{d}{dt}\left[\int_{V(t)} \phi dv\right] = \int_{V(t)} \frac{\partial \phi}{\partial t} dV + \int_{A(t)} \phi\left(\frac{d\mathbf{x}}{dt} \cdot \mathbf{n}\right) dA \tag{A.2}$$

to write (A.1) as

$$\frac{d}{dt}\int_{V(t)}\rho dV - \int_{A(t)}\rho\Big(\frac{d\mathbf{X}}{dt}\cdot\mathbf{n}\Big)dA + \int_{V(t)}\nabla(\rho\mathbf{V})dV \;=\; 0. \tag{A.3}$$

Using the divergence theorem to write the last term on the left of (A.3) as an integral over the area, we obtain

$$\frac{d}{dt}\int_{V(t)}\rho dV - \int_{A(t)}\rho\Big(\frac{d\mathbf{X}}{dt}\cdot\mathbf{n}\Big)dA + \int_{A(t)}\rho\mathbf{V}\cdot\mathbf{n}dA = 0. \tag{A.4}$$

If we consider $V(t)\to 0$ in such a way that $-\mathbf{n}_1 = \mathbf{n}_2 = \mathbf{n}$, the first term on the left of (A.4) vanishes and we obtain

$$\int_{A(t)}\rho_1\Big(\mathbf{V}\cdot\mathbf{n}_1 - \frac{d\mathbf{x}}{dt}\cdot\mathbf{n}_1\Big)dA \;+\; \int_{A(t)}\rho_2\Big(\mathbf{V}\cdot\mathbf{n}_2 - \frac{d\mathbf{x}}{dt}\cdot\mathbf{n}_2\Big)dA = 0, \tag{A.5}$$

giving us the conservation of mass flux (2.25).

In order to obtain (2.26) and (2.27), we multiply (2.16) by $\mathbf{V}$ add it to (2.11) and integrate over $V(t)$ to obtain

$$\int_{V(t)}\frac{\partial(\rho\mathbf{V})}{\partial t}dV + \int_{V(t)}\nabla(\rho\mathbf{V}\cdot\mathbf{V})dV = -\int_{V(t)}\nabla p dV. \tag{A.6}$$

Using (A.2) with the divergence theorem and letting $V(t)\to 0$ as we did before, we obtain

$$\int_{A(t)}\rho\mathbf{V}\Big(\mathbf{V}\cdot\mathbf{n} - \frac{d\mathbf{x}}{dt}\cdot\mathbf{n}\Big)dA + \int_{A(t)}p\mathbf{n}dA = 0. \tag{A.7}$$

Writing the velocity in terms of its normal and tangential components i.e.

$\mathbf{V} = \mathbf{V}\cdot\mathbf{n} + \mathbf{n}\times(\mathbf{V}\times\mathbf{n})$, we obtain (2.26) and (2.27).

APPENDIX B

DERIVATION OF THE RANKINE-HUGONIOT EQUATIONS AS A SINGULAR PERTURBATION PROBLEM

Following Matalon and Matkowsky [11], we are going to justify the Rankine-Hugoniot equations by matching solutions of the governing equations in the outer hydrodynamic zone and the inner thermal-diffusion zone of thickness $O(\delta)$, which contains a reaction zone of thickness $O(\epsilon\delta)$, as illustrated in Figure B.1.

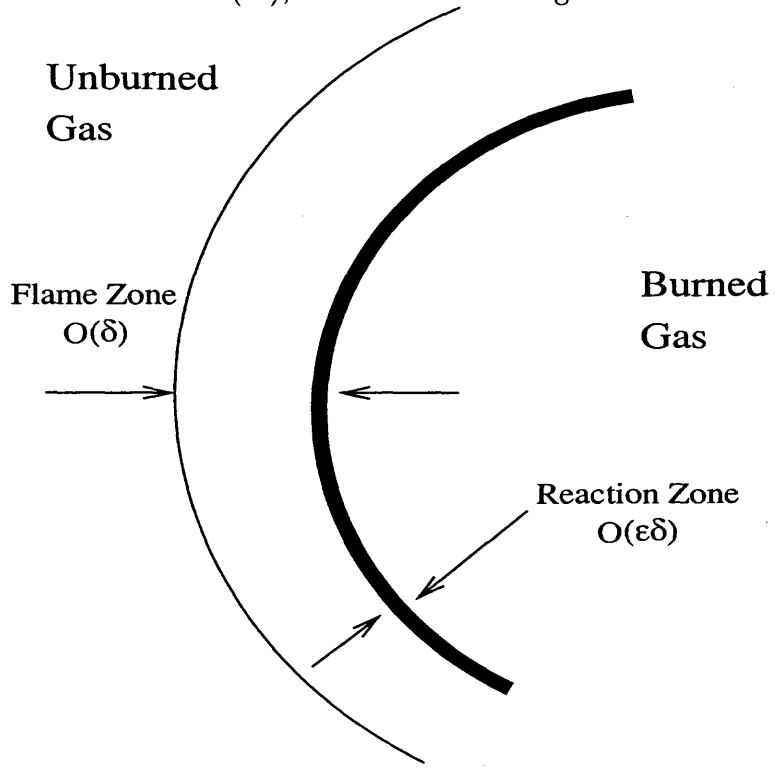

Figure B.1 Schematic representation of the various scales associated with a curved flame.

Solutions will be $O(1)$ solutions. The flame will be treated as a moving boundary layer. Results from the reaction zone , as done by Matkowsky and Sivashinsky [27], will be used. The flame surface will be described as

$$F(\mathbf{X}, t) = x - f(y, z, t). \tag{B.1}$$

We attach a moving coordinate system to the front $\xi = x - f(y, z, t)$, with the velocity in terms of its normal and tangential components $\mathbf{V} = u\mathbf{i} + \mathbf{v}$, with $\nabla = (\partial/\partial y, \partial/\partial z)$

and $s \equiv u - f_t - \mathbf{v}\cdot\nabla f$. Rewriting (2.11),(2.13), (2.16)–(2.18) in the moving coordinate system, we find the following,

$$\frac{\partial \rho}{\partial t} + \frac{\partial(\rho s)}{\partial \xi} + \nabla\cdot(\rho\mathbf{v}) = 0, \tag{B.2}$$

$$\rho\frac{\partial u}{\partial t} + \rho s\frac{\partial u}{\partial \xi} + \rho\mathbf{v}\cdot\nabla u = -\frac{\partial p}{\partial \xi} + \delta Pr\left\{\triangle u + \frac{1}{3}\frac{\partial}{\partial \xi}\left(\frac{\partial s}{\partial \xi} + \nabla\cdot\mathbf{v}\right)\right\}, \tag{B.3}$$

$$\begin{aligned}\rho\frac{\partial \mathbf{v}}{\partial t} + \rho s\frac{\partial \mathbf{v}}{\partial \xi} + \rho(\mathbf{v}\cdot\nabla)\mathbf{v} &= -\nabla p + \nabla f\frac{\partial p}{\partial \xi} \\ &+ \delta Pr\left\{\triangle\mathbf{v} + \frac{1}{3}\left(\nabla - \nabla f\frac{\partial}{\partial \xi}\right)\left(\frac{\partial s}{\partial \xi} + \nabla\cdot\mathbf{v}\right)\right\}\end{aligned} \tag{B.4}$$

$$\rho\frac{\partial Y}{\partial t} + \rho s\frac{\partial Y}{\partial \xi} + \rho\mathbf{v}\cdot\nabla Y - \delta Le^{-1}\triangle Y = -\delta\Omega \tag{B.5}$$

and

$$\rho\frac{\partial T}{\partial t} + \rho s\frac{\partial T}{\partial \xi} + \rho\mathbf{v}\cdot\nabla T - \delta\triangle T = -(\sigma-1)\delta\Omega. \tag{B.6}$$

If we consider flames where the mass and thermal diffusivities are nearly equal (appropriate for many of the flames we will be considering), we can write $Le = 1 + \epsilon\ell$ where ℓ is the deviation from unity of the Lewis number. We then combine (B.5) and (B.6) using the enthalpy $H \equiv T + (\sigma-1)Y$ to eliminate the reaction rate term, obtaining

$$\rho\frac{\partial H}{\partial t} + \rho s\frac{\partial H}{\partial \xi} + \rho\mathbf{v}\cdot\nabla H - \delta\triangle H = -\epsilon\delta\ell(\sigma-1)\triangle Y. \tag{B.7}$$

Given the smallness of the parameter δ, we will seek outer solutions denoted by capitals to (B.2)–(B.6), by considering expansions of the form,

$$\left.\begin{array}{ll} \theta = \Theta_0 + \delta\Theta_1 + \ldots, & h = H_0 + \delta H_1 + \ldots, \\ \rho = R_0 + \delta R_1 + \ldots, & s = S_0 + \delta S_1 + \ldots, \\ u = U_0 + \delta U_1 + \ldots, & \mathbf{v} = \mathbf{V}_0 + \delta\mathbf{V}_1 + \ldots, \\ p = P_0 + \delta P_1 + \ldots, & f = f^0 + \delta f^1 + \ldots. \end{array}\right\} \tag{B.8}$$

Substituting (B.8) into (B.2)-(B.7) we find the resulting equations to $O(1)$ are

$$\frac{\partial \Theta_0}{\partial t} + S_0 \frac{\partial \Theta_0}{\partial \xi} + \mathbf{V}_0 \cdot \nabla \Theta_0 = 0 \tag{B.9}$$

and

$$\frac{\partial H_0}{\partial t} + S_0 \frac{\partial H_0}{\partial \xi} + \mathbf{V}_0 \cdot \nabla H_0 = 0. \tag{B.10}$$

The flow field satisfies Euler's equations

$$\frac{\partial S_0}{\partial t} + \nabla \cdot \mathbf{V}_0 = 0, \tag{B.11}$$

$$R_0 \left(\frac{\partial U_0}{\partial t} + S_0 \frac{\partial U_0}{\partial \xi} + \mathbf{V}_0 \cdot \nabla U_0 \right) = -\frac{\partial P_0}{\partial \xi} \tag{B.12}$$

and

$$R_0 \left(\frac{\partial \mathbf{V}_0}{\partial t} + S_0 \frac{\partial \mathbf{V}_0}{\partial \xi} + (\mathbf{V}_0 \cdot \nabla)\mathbf{V}_0 \right) = -\nabla P_0 + \nabla f^0 \frac{\partial P_0}{\partial \xi} \tag{B.13}$$

and the flame speed becomes

$$S_0 = U_0 - f_t^0 - \mathbf{V}_0 \cdot \nabla f^0. \tag{B.14}$$

Using (B.2) and integrating (B.3) and (B.4) across ξ, we find the following jump conditions for the reaction zone

$$[s] = [u] = [\mathbf{v}] = 0. \tag{B.15}$$

Multiplying (B.3) by ∇f^0 adding it to (B.4) then integrating across ξ we find

$$\left[\frac{\partial \mathbf{v}}{\partial \xi} + \nabla f^0 \frac{\partial u}{\partial \xi} \right] = 0. \tag{B.16}$$

In addition to (B.15) and (B.16), we also use from the reaction zone analysis of Matkowsky and Sivashinsky [27]

$$[\theta] = [h] = 0, \tag{B.17}$$

$$\delta\sqrt{(1+|\nabla f|^2)}\left[\frac{\partial\theta}{\partial\xi}\right] = -(\sigma-1)e^{\frac{1}{2}h(0,y,z,t)} \tag{B.18}$$

and

$$\left[\frac{\partial h}{\partial\xi}\right] = -\ell\left[\frac{\partial\theta}{\partial\xi}\right]. \tag{B.19}$$

In order to do the local analysis, we introduce the stretching transformation $\xi = \delta\zeta$ and seek inner expansions of the form

$$\left.\begin{array}{ll} \theta = \theta_0 + \delta\theta_1 + \ldots, & h = h_0 + \delta h_1 + \ldots, \\ \rho = \rho_0 + \delta\rho_1 + \ldots, & s = s_0 + \delta s_1 + \ldots, \\ u = u_0 + \delta u_1 + \ldots, & \mathbf{v} = \mathbf{v}_0 + \delta\mathbf{v}_1 + \ldots, \\ p = p_0 + \delta p_1 + \ldots, & m = m_0 + \delta m_1 + \ldots. \end{array}\right\} \tag{B.20}$$

Using (B.20) in (B.2)–(B.7) with the stretched variable ζ we find to lowest order

$$\frac{\partial m_0}{\partial\zeta} = 0, \tag{B.21}$$

$$m_0\frac{\partial\theta_0}{\partial\zeta} - (1+|\nabla f^0|^2)\frac{\partial^2\theta_0}{\partial\zeta^2} = 0, \tag{B.22}$$

$$m_0\frac{\partial h_0}{\partial\zeta} - (1+|\nabla f^0|^2)\frac{\partial^2 h_0}{\partial\zeta^2} = \ell(1+|\nabla f^0|^2)\frac{\partial^2\theta_0}{\partial\zeta^2}, \tag{B.23}$$

$$m_0\frac{\partial u_0}{\partial\zeta} - Pr\left\{(1+|\nabla f^0|^2)\frac{\partial^2 u_0}{\partial\zeta^2} + \frac{1}{3}\frac{\partial^2 s_0}{\partial\zeta^2}\right\} = -\frac{\partial p_0}{\partial\zeta}, \tag{B.24}$$

$$m_0\frac{\partial\mathbf{v}_0}{\partial\zeta} - Pr\left\{(1+|\nabla f^0|^2)\frac{\partial^2\mathbf{v}_0}{\partial\zeta^2} - \frac{1}{3}\frac{\partial^2 s_0}{\partial\zeta^2}\nabla f^0\right\} = \nabla f^0\frac{\partial p_0}{\partial\zeta}, \tag{B.25}$$

$$s_0 = u_0 - f_t^0 - \mathbf{v}_0\cdot\nabla f^0, \tag{B.26}$$

$$m_0 = \rho_0 s_0, \qquad \rho_0\theta_0 = 1. \tag{B.27}$$

Using (B.21) we solve (B.22) and (B.23) since $m_0 = m_0(y,z,t)$ to obtain leading order solutions for θ and h

$$\theta_0 = \begin{cases} 1+(\sigma-1)e^{\zeta/m_0} & \zeta < 0 \\ \sigma & \zeta > 0, \end{cases} \tag{B.28}$$

$$h_0 = \begin{cases} -\ell(\sigma-1)m_0^{-1}\zeta e^{\zeta/m_0} & \zeta < 0 \\ 0 & \zeta > 0. \end{cases} \tag{B.29}$$

In order to satisfy (B.17) and (B.18), we require

$$m_0 = \sqrt{1+|\nabla f^0|^2} \tag{B.30}$$

for $\zeta < 0$. With $\rho = 1$ and from (2.11) we justify Landau's assumption obtaining $S_f = \frac{s_0}{\sqrt{1+|\nabla f|^2}} = 1$. To calculate u_0 and $\mathbf{v}_0$, we combine (B.24) and (B.25) to obtain

$$\frac{1}{Pr\ m_0}\frac{\partial(u_0\nabla f + \mathbf{v}_0)}{\partial\zeta} - \frac{\partial^2(u_0\nabla f + \mathbf{v}_0)}{\partial\zeta^2} = 0. \tag{B.31}$$

The jump condition (B.16) implies that $\mathbf{v}_0 + u_0\nabla f^0$ has continuous derivatives at $\zeta = 0$ and is independent of ζ. The solutions to (B.31) are constants with respect to ζ, by matching to the outer solutions we find

$$u_0 = \begin{cases} U_0(0^-,y,z,t) + ((\sigma-1)/m_0)e^{\zeta/m_0} & \zeta < 0 \\ U_0(0^-,y,z,t) + (\sigma-1)/m_0 & \zeta > 0, \end{cases} \tag{B.32}$$

$$\mathbf{v}_0 = \begin{cases} \mathbf{V}_0(0^-,y,z,t) - \nabla f^0((\sigma-1)/m_0)e^{\zeta/m_0} & \zeta < 0 \\ \mathbf{V}_0(0^-,y,z,t) - \nabla f^0((\sigma-1)/m_0) & \zeta > 0. \end{cases} \tag{B.33}$$

and

$$p_0 = \begin{cases} P_0(0^-,y,z,t) + (\frac{4}{3}Pr-1)(\sigma-1)e^{\zeta/m_0} & \zeta < 0 \\ P_0(0^-,y,z,t) - (\sigma-1) & \zeta > 0. \end{cases} \tag{B.34}$$

Using (B.32)–(B.34), we can the write the jump conditions across the flame zone as,

$$[U_0] = (\sigma-1)\frac{1}{\sqrt{(1+|\nabla f^0|^2)}}, \tag{B.35}$$

$$[\mathbf{V}_0 + U_0\nabla f^0] = 0 \tag{B.36}$$

and

$$[P_0] = -(\sigma-1). \tag{B.37}$$

Using (B.35) and (B.36), we obtain (2.25) and (2.26) respectively and combining (B.35) with (B.37) we obtain (2.27).

APPENDIX C

J_I AND J_I'

C.1 J_i and J_i' for the Spherically Expanding Flame

$$J_1' = (2\alpha - \ell_c(\sigma-1)^2 I_2)\,[\sigma\omega - (n+1)\alpha_1] \tag{C.1}$$

$$J_1 = -\left[3(\sigma-1)^2\sigma\ell_c I_2 - 2\alpha\sigma\right] - \alpha\Gamma_1 \tag{C.2}$$

$$J_2' = -\omega\left(\ell_c(\sigma-1)^2 - 2\alpha\right)\left[\alpha_2 + \frac{n\alpha_3}{\omega-n} - \sigma\right] \tag{C.3}$$

$$\begin{aligned} J_2 &= \left(\ell_c(\sigma-1)^2 I_2 - 2\alpha\right)\left[\frac{\alpha_3 n^2}{(\omega-n)^2}(\omega-n+1) + \sigma\right] \\ &- \lambda_+ Pr\Gamma_2 - \sigma\left[(\sigma-1)I_1 - \alpha\right]\kappa \end{aligned} \tag{C.4}$$

$$J_3' = -\left(\ell_c(\sigma-1)^2 I_2 - 2\alpha\right)\left[\alpha_1 + \frac{\omega(\omega+2)\alpha_2}{n(n+1)} + \frac{\omega\alpha_3}{\omega-n}\right] \tag{C.5}$$

$$\begin{aligned} J_3 &= \ell_c(\sigma-1)^2\sigma I_2 + \left(\ell_c(\sigma-1)^2 I_2 - 2\alpha\right)\frac{n(\omega-n+1)}{(\omega-n)^2}\alpha_3 \\ &- \frac{\omega(\omega^2+3\omega+2-n(n+1))}{n(n+1)}\alpha_2\lambda_+ Pr \\ &- (\lambda_+ Pr + \sigma I_1)\left[3(\sigma-1) + \frac{\omega(\omega+2)}{n(n+1)}\alpha_2 - (n-1)\alpha_3 + (n+2)\alpha_1\right] \\ &+ (\lambda_+ - 1)Pr\left[(n+2)\alpha_1 + 3(\sigma-1)\right] \end{aligned} \tag{C.6}$$

$$J_4' = (n+1)\alpha_1\left(\ell_c(\sigma-1)^2 I_2 - 2\alpha\right) \tag{C.7}$$

$$\begin{aligned} J_4 &= 2\sigma(n+1)\alpha\alpha_1 - (\sigma-1)\sigma\left(\ell_c(1-\sigma)\sigma I_2 - 4\alpha\right) \\ &- \sigma I_1\left(\alpha_3(\omega-n+1)n - \alpha_1(n+1)\left[\sigma(\omega+1) + \sigma(n+1) - (\sigma-1)(n+4)\right] + 2(\sigma-1)(3igm\right. \\ &+ (\sigma I_1 + I_3)(n+2)(n-1) \\ &- Pr\left[2(I_3-\lambda_+)(n+2)(n-1) - (\lambda_+-1)(2(\sigma-1) + (n+1)(n+2)\alpha_1\right] \\ &+ \left[u^*\alpha - (\sigma-1)\sigma I_1\right]\Gamma_1 \end{aligned}$$

REFERENCES

1. M. Izumikawa, T. Mitani and T. Nioka, *Experimental Study on Cellular Flame Propagation of Blend Fuels*, Combust. Flame, 73 (1988), pp. 207–214

2. E. von Lavante and R. A. Strehlow, *The Mechanism of Lean Limit Flame Extinction* Combust. Flame 49 (1983) pp. 123–140

3. E. G. Groff, *The Cellular Nature of Confined Spherical Propane-Air Flames*, Combust. Flame, 48 (1982), pp. 51–62.

4. D. M. Simon and E. L. Wong, *Burning Velocity Measurement*, J. Chem. Phys., 21 (1953), pg. 936.

5. C. D. Lind and J. C. Whitson, *Explosive Hazards Associated with Spills of Large Quantities of Hazardous Materials*, D.O.T. US Coast Guard Final Rep. ADA-047585, 1977

6. P. F. Ivashchenko and V.S. Rumyantsev, *Convective Lift and the Propagation Velocity of a Large Fire Cell* Fiz Goreniya Vzryva, 40 (1978), pp. 83–87.

7. L. D. Landau, *On the Theory of Slow Combustion*, Acta Physicochimica URSS, 73 (1944), pp. 77–85.

8. G. Darrieus, *Propagation d'un Front de Flamme: Assai de Théorie des Vitesses Anomales de Déflagration par développement Spontané de la Turbulence*, Presented at the Int. Congr. Appl. Mech., 6th., Paris, 1946

9. A. G. Istratov and V. B. Librovich, *On the Stability of Gasdynamic Discontinuities Associated with Chemical Reactions. The Case of a Spherical Flame*, Astronautica Acta., 14 (1969), pp. 453–467.

10. G. H. Markstein, *Experimental and Theoretical Studies of Flame-Front Stability*, Journal of the Aeronautical Sciences, March (1951), pp. 199–209.

11. M. Matalon and B. J. Matowsky, *Flames as Gas Dynamic Discontinuities*, J.Fluid Mech., 124 (1982), pp. 239–259.

12. P. Clavin and F. A. Williams, *Effects of Molecular Diffusion and of Thermal Expansion on the Structure and Dynamics of Premixed FLames in Turbulent Flows of Large Scale and Low Intensity*, J. Fluid Mech., 116 (1982), pp. 251–282.

13. M. L. Frankel and G. I. Sivashinsky, *The Effect of Viscosity on Hydrodynamic Stability of a Plane Flame Front*, Comb. Sci. Technol., 29 (1982), pp. 207–224.

14. M. Matalon and B. J. Matkowsky, *On the Stability of Plane and Curved Flames*, SIAM J. APPL. MATH., 44 (1984) pp. 327–343.

15. P. Pelce and P. Clavin, *Influence of Hydrodynamics and Diffusion Upon the Stability Limits of Laminar Premixed Flames*, J. Fluid Mech., 124 (1982), pp. 219–237.

16. J. K. Bechtold and M. Matalon, *Hydrodynamic and Diffusion Effects on the Stability of Spherically Expanding Flames*, Combust. Flame., 67 (1987), pp. 77–90.

17. D. Bradley and C. M. Harper., *The Development of Instabilities in Laminar Explosion Flames*, Combust. Flame., 99 (1994), pp. 562–572.

18. D. Bradley, C. G. W. Sheppard, R. Woolley, D. A. Greenhalgh and R. D. Lockett, *The Development and Structure of Flame Instabilities and Cellularity at Low Markstein Numbers in Explosions*, Combust. Flame, 122 (2000), pp. 195–209.

19. D. Bradley, *How Fast Can We Burn?*, Twenty-Fourth Symposium (International) on Combustion/ The Combustion Insitute, (1992), pp.247–262.

20. Bradley, D.K., *Instabilities and Flame Speeds in Large-Scale Premixed Gaseous Explosions*, Phil. Trans. R. Soc. Lond. A, 357 (1999) pp. 3567–3581.

21. J. K. Bechtold and M. Matalon, *Marstein Numbers for Near-Stoichiometric Flames with Variable Transport Properties*, To appear

22. T. L. Jackson, *Effect of Thermal Expansion on the Stability of Two-Reactant Flames*, Combust. Sci. Tech., 53 (1987), pp. 51–54.

23. P. L. Garcia-Ybara and P. Clavin, *Cross Transport Effects in Nonadiabatic Premixed Flame.*, Prog. Aeronautics Astronautics, 76 (1981) pp. 463–481.

24. G. I. Sivashinsky, *On a Converging Spherical Flame Front*, Int. J. Heat Mass Transfer, 17 (1974), pp. 1499–1506.

25. C. J. Sun and C. K. Law, *On the Consumption of Fuel Pockets Via Inwarly Propagating Flames*, Twenty-Seventh Symposium (International) on Combustion, (1988) pp. 963–970.

26. C. J. Sung, C. J. Sun and C. K. Law, *Linear Stability Analysis of Inwardly-Propagating Spherical Flames*, CST Comm. 1 (2000) pp. 7–10.

27. B. J. Matkowsky and G. I. Sivashinsky, *An Assymptotic Derivation of Two Models in Flame Theory Associated with the Constant Density Approximation*, SIAM J. Appl. Math., 37 (1979), pp. 686–699.

28. B. Karlovitz, D. W. Denniston, D. H. Knapschaefer and F. H. Wells, *Studies on Turbulent Flames*, Fourth (International) Symposium on Combustion 613–620 (1953)

29. Y. D. Kim and M. Matalon, *Propagation and Extinction of A Flame in a Stagnation-Point Flow* Combust. Flame, 73 (1988) pp. 303–313.

30. W. F. Williams, *Combustion Theory*, Addison-Wesley, (1985)

31. Strehlow, R.A., *Fundamentals of Combustion*, International Textbook Company, (1968)

32. Matalon, M., and Bechtold, J.K., *Proceedings of the 1987 ASME/JSME Thermal Engineering Joint Conference* **1**: 95–101 (1987)

33. M. Matalon and B. J. Matkowsky, *Flames in Fluids: Their Interaction and Stability*, Comb. Sci. Technol., 34 (1983). pp. 295–316.

34. H. S. Mukunda and J. P. Drummond, *Two Dimensional Linear Stability of Premixed Flames Under Zero Gravity*, Applied Scientific Research, 51 (1993), pp. 687–711.

35. J. Manton, G. von Elbe and B. Lewis, *Nonisotropic Propagation of Combustion Waves in Explosive Gas Mixtures and the Development of Cellular Flames*, Journal of Chemical Physics, 20 (1952), pp. 153–157.

36. B. Bregeon, A. S. Gordon and F. A. Williams, *Near-Limit Downward Propagation of Hydrogen and Methane Flames in Oxygen-Nitrogen Mixtures*, Combust. Flame, 33 (1978), pp. 33–45.

37. Yu. A. Gostintsev, A. G. Istratov and Yu. V. Shulenin, *Self-Similiar Propagation of a Free Turbulent Flame in Mixed Gas Mixtures*, Combust. Explosion and Shock Waves, March (1988), pp. 563–569.

38. L. Filyand, G. I. Sivashinsky and M. L. Frankel, *On Self-Acceleration of Outward Propagating Wrinkeled Flames*, Physica D, 72 (1994) pp. 110–118.

39. M. Matalon, C. Cui and J. K. Bechtold, *Hydrodynamic Theory of Near-Stoichiometric Premixed Flames* In Preperation

40. D. Bradley, R. A. Hicks, M. Lawes, C. G. W. Sheppard and R. Woolley, *The Measurement of Laminar Burning Velocities and Markstein Numbers fo Iso-octane-n-Heptane-Air Mixtures at Elevated Temperatures and Pressures in an Explosion Bomb*, Combust. Flame, 115 (1998), pp. 126–144.